NUMERICAL AND EXPERIMENTAL EVALUATION OF THE EFFECT OF AN OVERSIZE PARTICLE ON DIRECT SHEAR TEST RESULTS

by
Hooman Hosseinpour

A Thesis Submitted in Partial Satisfaction of the
Requirements for the Degree of
Master of Science

in

Mineral Engineering
with Emphasis in
Geotechnical Engineering

in the
GRADUATE DIVISION
of the
NEW MEXICO INSTITUTE of MINING and TECHNOLOGY

August 2008

NUMERICAL AND EXPERIMENTAL EVALUATION OF THE EFFECT OF AN OVERSIZE PARTICLE ON DIRECT SHEAR TEST RESULTS

By

Hooman Hosseinpour

To my parents
for letting me pursue my dream
so far from home

&

To my dear sister, brother in law, and lovely nephew
who are always in my heart

I would like to express my special appreciation
to my dear mother
and respectfully dedicate this thesis to her
who has dedicated herself for educating and advising many people and
was my first teacher in class inspiring me in learning and discovering
the wonderful world

"Problems should be as simple as possible, but not simpler."

Albert Einstein

ABSTRACT

Numerical and Experimental Evaluation of the Effect of an Oversize Particle on Direct Shear Test Results

by

Hooman Hosseinpour

Master of Science in Mining engineering
with Emphasis in Geotechnical Engineering

New Mexico Institute of Mining & Technology

Advisor: Dr. Ali Fakhimi

From 1969 to 1982 approximately 320 million tons of overburden material were removed from the Questa open-pit mine and deposited onto mountain slopes, making nine rock piles. In the course of a multi-disciplinary investigation on the effect of weathering on the long-term gravitational stability of rock piles, several *in-situ* shear tests were conducted on the rock pile materials. Such materials have a wide range of particle sizes, including large rock fragments observed in the blocks of rock pile material that underwent in-situ shear testing. Because large rock fragments were found in the shear box that can affect the results of the shear tests, the role of oversize particles on the shear strength of Questa rock pile material was investigated using both experimental and numerical techniques.

Several laboratory direct shear tests using a 6 cm × 6 cm shear box were performed in which the size and location of an oversize particle were changed in the shear box. Through this endeavor, it was found that in addition to the size, the location of the oversize particle is an important parameter that can affect the measured shear strength of the rock pile material. Following the experimental study, numerical modeling of the laboratory direct shear box was performed to observe the effective parameters that are not easily detected or measured in the laboratory. For this purpose,

the hybrid finite-discrete element computer code (CA2) was used. It was observed that the numerical simulation of the laboratory direct shear box can provide consistent results with those obtained in the laboratory and can successfully mimic the behavior of the laboratory direct shear box. Both the laboratory direct shear tests and the numerical model have shown that the presence of an oversize particle cause an increase in friction angle while the cohesion intercept can either decrease or increase depending on the location and size of the oversize particle with respect to the size of direct shear box.

The 60 cm × 60 cm *in-situ* direct shear box that was used in the field testing was modeled numerically to determine the effect of an oversize particle on shear strength. It was noted that the friction angle and cohesion intercept calculated in the *in-situ* test model are less affected by the presence and location of an oversize particle than in the laboratory direct shear box tests. This is due to the construction of the *in-situ* shear box as a half a box; the second half is made of earth material that is theoretically infinite in size. Therefore, the oversize particle should not be considered oversized as it is in the laboratory test. Consequently, the effect of an oversize particle in the *in-situ* shear test simulation causes changes in cohesion intercept and friction angle that are due more to chaotic nature of the discrete system rather than the systematic well-defined changes in shear strength that are observed in simulation of the conventional laboratory shear box.

Considering all the experimental and numerical direct shear tests results, it is concluded that the ASTM requirement regarding the maximum permissible particle size in a laboratory direct shear test is too conservative for the Questa rock pile material and the range of normal stresses used in this study. A ratio of 0.2 of the maximum particle size diameter to the box width is recommended, resulting in only

minor error in the measured cohesion and friction angle of Questa mine rock pile material.

Acknowledgements

For his continued guidance, support, and encouragement throughout my studies at New Mexico Institute of Mining and Technology, I would like to offer my sincere thanks to my advisor, Dr. Ali Fakhimi, whose valuable advice helped me to conduct this research study during my Master's degree. My special thanks to him for being generous in his time although his free time has been very tight. In addition, I am so grateful to my committee members who have been so supportive. Dr. Navid Mojtabai, department chair, who provided me with his great advice during my studies at New Mexico Tech. Dr. Mehrdad Razavi who has inspired me in my field of interest and always encouraged me in resolving the difficulties. He provided me with his computer program written in MATLAB, which helped me to make some animations of my computer model for interpretation of the results. Dr. Claudia Wilson whose structural dynamics class inspired me in my field of interest. Her teaching style is indeed unforgettable, especially considering the fact that her class was the first class I experienced in the United States. She always supported and encouraged me and generously dedicated her time in order to answer all my questions. I would like to thank Dr. Virginia McLemore for her advice and support during the course of this research.

I would like to thank my colleagues and friends at NMTech with whom I have had a pleasure of working over these two years. These include Shantanu Tiwari, Kwaku Boakye, John Morkeh, Samuel Nunoo, and all other graduate students involved in the Questa Weathering and Stability project.

This research study was supported by Chevron Mining Inc. (formerly Molycorp, Inc.) in the form of a Research Assistantship by New Mexico Bureau of Geology and Mineral Resources and New Mexico Institute of Mining and Technology, which is highly appreciated. I am also grateful to Dr. David Jacobs from Chevron Mining Inc. for his encouragement and providing me with great comments pertaining to my thesis.

I also would like to remind my great advisor during my undergraduate studies, the late Professor Sirous Zarayan, The Father of Contemporary Geology of Iran, whose encouragements and great advice would remain in my brain and heart forever.

Last and definitely the most, I want to offer my sincere thanks and appreciation to my dear family. In fact, words cannot express my thanks to them who always encouraged me and helped me continuing my education. I am so thankful for their kind thoughts and wishes.

TABLE OF CONTENTS

LIST OF FIGURES

CHAPTER 1
Introduction

1. Background

The Questa molybdenum mine, owned and operated by Chevron Mining Inc. (formerly Molycorp, Inc.), is located on the western slope of the Taos Range of the Sangre de Cristo Mountains of the Southern Rocky Mountains near the edge of the Rio Grande rift in north-central New Mexico, USA (Figure 1). The mine is on southward facing slopes and is bounded on the south by Red River (elevation of approximately 2280 m) and on the north by the mountain divides (elevation approximately 3270 m). During the period of open-pit mining (1969-1982), approximately 320 million tones of overburden (non-ore) rock were removed and deposited onto mountain slopes and into tributary valleys forming nine rock piles flanking the open-pit mine. The rock piles were formed at an angle of repose of approximately 37º using end-dumping methods (Gutierrez, 2006). These are some of the highest rock piles in the United States. Since the rock piles were emplaced, a foundation failure occurred at Goathill North rock pile that resulted in slumping of the rock pile since its construction (Gutierrez, 2006). The end-dumping construction method resulted in the stratified, layered rock piles that allows movement of air and

water vapor through the unsaturated rock piles affecting their long term oxidation, acid mine drainage, and slope stability.

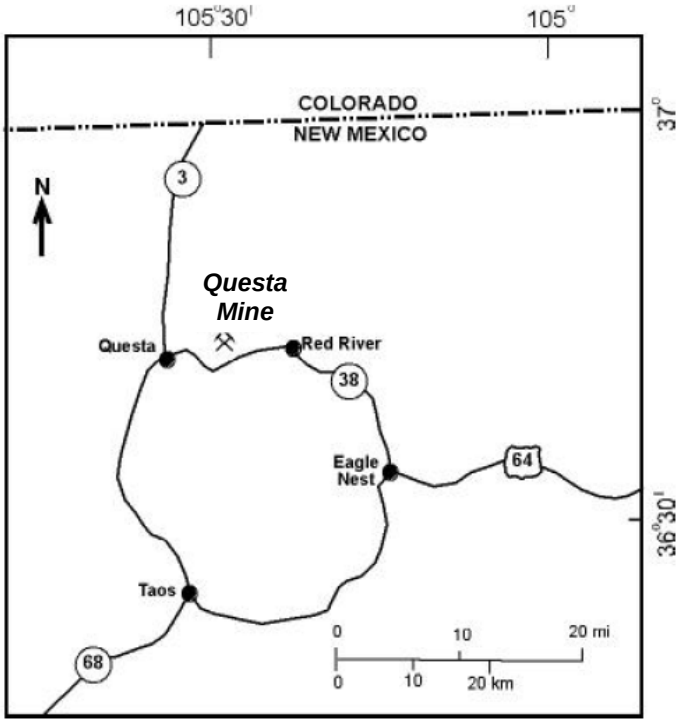

Figure 1: Location of the Questa Mine.

A multi-disciplinary, independent research team of academicians and consultants was contracted by Chevron Mining, Inc. to investigate the effect of weathering on the long-term gravitational stability of the rock piles. As part of this research work, *in-situ* shear boxes 30 cm × 30 cm and 60 cm × 60 cm in size were designed (Fakhimi, et al., 2008) and used to obtain the cohesion intercept and friction angle of the rock pile material. During the course of *in-situ* testing, oversize rock fragments were encountered in the rock pile. The purpose of this research is to study the effect of an oversize particle on the deformational and strength properties of Questa rock pile material.

2. Problem Statement

In order to measure the cohesion and friction angle of Questa rock pile material, several *in-situ* direct shear tests were conducted. During the *in-situ* direct shear testing, large rock fragments were encountered in the shear box block of tested rock pile material. These large rock fragments can modify the shear strength and deformational characteristics of the material. The literature review shows that only a few research studies with emphasis on the effect of scalping on the mechanical behavior of rock fill dam material have been conducted. However, there is not a general agreement among researchers on the effect of oversize particles on direct shear test results. In fact, some studies show that oversize particles can increase the friction angle of soil, while there have been some other researches with opposite conclusions indicating reduction in the measured friction angle due to presence of oversize particles in the shear box. Furthermore, it appears that there has not been any specific study on the effect of a single oversize particle on the cohesion and friction angle of rock pile materials.

To study the role of an oversize particle on the measured friction angles and cohesions of *in-situ* direct shear tests, laboratory experiments and numerical modeling were conducted on the unsaturated samples of the rock pile material. In the experimental study, a 6 cm × 6 cm shear box in size was used. The oversize particles were simulated using stainless steel spheres in three different sizes that were placed along the shear plane. In order to investigate the effect of the location of oversize particle in shear box, sensitivity analyses were performed by changing the location of oversize particle along the shear band. For this purpose, the oversize particles were placed at the center and on the left and right sides of the shear box. In the numerical simulation, a hybrid discrete-finite element method was implemented in which the

rock pile material was modeled with discrete particles while the shear box was modeled with finite elements.

3. Literature Review

The presence of oversize particles in a soil sample can change the results of direct shear tests. This subject has been of particular interest in testing of rock fill materials since small shear boxes or triaxial cells were intended to be used for testing these materials after scalping or removal of large rock fragments from the sample tested. The removal of oversize particles can modify the soil matrix and consequently its shear strength.

Hennes (1952) studied the effect of particle size, shape, and grading on the friction angle of dry, rounded gravel, and crushed rock. The shear test apparatus was 152.4 mm × 304.8 mm (6-inch × 12-inch) in size. He concluded that as the maximum particle size increased, the friction angle increased. Note that in Hennes's research work, the samples were compacted following identical vibration and tapping of the material without verifying the resulting porosity of the samples.

Holtz and Gibbs (1956) conducted several triaxial tests on river sand and gravel and quarry material to investigate the effect of density, maximum particle size, particle shape, and amount of gravel on the shear strength of the material. All samples were saturated before testing and the loading rate was slow enough to allow free drainage of the material without generating any excess pore water pressure. Samples with 70% relative density that contained 0%, 20%, 35%, 50%, and 65% gravel were tested to investigate the effect of percentage of gravel on the shear strength. The friction coefficients were 0.72, 0.76, 0.81, 0.84, and 0.78, respectively. The friction angle increased as the percentage of gravel was increased up to a gravel content of

50% and then started to decrease, which could be because of less well-graded material in the latter situation as was proposed by the authors. The effect of maximum particle size was investigated by these authors as well. Large samples (228.6 mm × 571.5 mm) with 20% gravel content placed at 70% relative density were tested. The failure envelopes for minus 19.05 mm, 38.1 mm, and 76.2 mm maximum particle size (ratios of maximum particle size to the sample diameter of 0.083, 0.167, and 0.333) were practically identical. A similar conclusion was obtained as the percentage of the gravel was increased to 50%. The authors suggested that the large particles in these experiments caused little increase in friction coefficient because only a few large particles existed in the tested materials.

Rathee (1981) in his study of granular soils, using a 30 cm × 30 cm shear box and maximum applied normal stress of about 300 kPa, concluded that the ratio of sample width to maximum particle size that does not affect the shear strength is in the order of 10 to 12 for sand-gravel mixture. Based on this author, the friction angle of sand-gravel mixture increases with the increase in the maximum particle size while for almost uniform size gravel, the friction angle was almost constant with increasing the maximum particle size.

Cerato and Lutenegger (2006) studied the scale effect of direct shear tests on sands. Their study showed that the friction angle measured by direct shear testing can depend on sample size and that the influence of sample size is also a function of sand type and relative density. They concluded that for dense sand, the friction angle measured by direct shear testing reduced as the box size increased and that a box width to maximum particle size ratio of 50 or larger should be used in order to minimize the size effect on the friction angle of sand. Furthermore, these authors

claimed that the thickness of shear zone in a direct shear test is not only a function of the mean particle size (D_{50}), but also depends upon the height and width of the box.

Su (1989) performed triaxial testing and suggested that static strength of a soil with oversize particles in the floating state is mainly determined by the soil matrix in the far field. Tests should be performed on the soil matrix alone at the dry density of far field matrix to obtain the shear strength of the soil with the floating oversize particles.

Through direct shear testing on sand and gravel, Simoni and Houlsby (2006) showed that the addition of gravel to the mixture causes an increase in peak and constant volume friction angles.

The above researches illustrated no change or increase in friction angle with the increase in the maximum particle size or the ratio of maximum particle size to the box width. On the other hand, there have been some reports that suggest reduction in friction angle with increase in particle size. For example, Becker et al. (1972) used a biaxial apparatus to measure the friction angle of earth dam material in a plane strain condition. They concluded that in general the friction angle decreases as the maximum particle size increases but the difference in friction angle between the small size material and the large size material diminishes as the confining pressure increases.

Nieble et al. (1974) conducted direct shear tests on uniform crushed basalt and showed that as the maximum particle size increases, the friction angle decreases. His study showed that a maximum particle size less than 5% of the shear box width should be used to avoid size effect in measuring the friction angle.

Kirkpatrick (1965), having studied the Leighton Buzzard sand with uniform particle sizes, using triaxial tests, showed reduction in friction angle as the mean particle size was increased while the porosity was kept a fixed value.

Large triaxial tests on gravelly soils with parallel straight-line grading curves and maximum particle sizes of minus sieve No. 10, 6.35 mm, 12.7 mm, 25.4 mm, and 50.8 mm were conducted by Leslie (1963). All gradings had a uniformity coefficient of 3.3. Based on these series of tests, Leslie concluded that the intermediate particle sizes rather than the large particles had a greater influence on the shear strength and that the influence of oversize particles may not be as important as was suspected.

To eliminate or reduce the effect of oversize particles on the shear strength, ASTM standard D3080-98 (2003) recommends that the maximum particle size in a shear test must be no larger than one tenth of the shear box width and one sixth of the box height.

The above literature review suggests that there is not a consensus among the researchers on the role of oversize particles on the results of direct shear tests. Furthermore, the issue of presence of just one oversize particle in a sample of rock pile material does not seem to have been addressed. In fact, the focus of past research has been to study how the friction angle changes as many oversize particles are removed from rock fill material samples.

3. Thesis Outline

This thesis consists of five chapters. In this first chapter, the background, the objective of the research work, and the literature review are discussed.

Chapter 2 presents experimental part of this research study that includes laboratory direct shear tests of Questa mine rock pile material. In this chapter, I

explain whether or not an oversize particle can change the strength and deformational behavior of soil material. In addition, the effect of location of an oversize particle on strength and deformational characteristics of the material is discussed. For this purpose, steel spheres with diameter of 0.66 cm, 1.28 cm, and 1.90 cm are used to simulate the oversize particles. In order to investigate the effect of location of oversize particles, the steel spheres are placed at three different locations along the shear band namely at the center, and on the left and right sides of the box.

Chapter 3 presents the numerical simulation of the laboratory direct shear box. The computer program CA2 (Fakhimi, 1998) that is a hybrid finite-discrete element code was used for this study. The history of several parameters such as the shear stress, shear displacement, and normal displacement of the simulated soil sample was investigated in detail. The oversize particles in the numerical model were simulated with circular cylinders that similar to the experimental studies were accommodated at different locations along the shear band in the shear box. The results of numerical simulations are discussed in detail. In particular, it is shown how the deformation pattern and the micromechanical damages help to understand the role of oversize particles on the mechanical behavior of the material.

Chapter 4 aims to simulates the *in-situ* shear box tests by numerical modeling. Similar to the laboratory test simulations, cylindrical particles were used as oversize particles in the simulations.

I finally conclude in Chapter 5 by considering all the experimental and numerical results obtained from the laboratory and *in-situ* tests. It is concluded that the presence of an oversize particle in the shear box can modify the shear strength and deformational behavior of the soil material. In addition, it is concluded that the location of the oversize particle is important in the measured friction angle and

cohesion. Finally, it is shown that for the Questa mine rock pile material and the range of normal stresses used in this study, the general recommendation proposed by ASTM for the maximum allowable particle size in a shear box can be somewhat relaxed. In particular, a maximum particle size equal to 20% of box width seems to be applicable in a direct shear test without causing a significant error in the measured friction angle and cohesion.

CHAPTER 2
Laboratory Testing

1. Introduction

In this chapter, laboratory direct shear tests on Questa rock pile material are discussed. Laboratory shear tests with oversize stainless steel balls were conducted as these tests are much easier to perform and less expensive compared to the *in-situ* shear tests. The results of these laboratory tests were used to verify the accuracy of the numerical model discussed in the next chapter. After verification of the numerical model, the model was applied for simulation of *in-situ* shear tests with greater confidence. Numerical simulation of *in-situ* shear tests helped us to understand the role of oversize particles on the shear strength of the Questa rock pile material in detail.

2. Direct Shear Test

2-1. Shear Strength of Soil

Shear strength of a soil sample is its internal strength per unit area against shear failure.

2-2. Mohr-Coulomb Failure Criterion

In 1900, Mohr proposed a hypothesis for failure of a material. He mentioned that a material fails if it is exposed to a critical combination of normal and shear stresses simultaneously (Das, 1985). Based on this theory, the relationship between normal (σ) and shear stresses (τ_f) on failure plane was proposed as follows:

$$\tau_f = f(\sigma) \tag{1}$$

The failure envelope is defined by the above equation. In majority of situations, equation (1) is assumed to be linear (Mohr-Coulomb failure criterion) that is defined by:

$$\tau_f = c + \sigma.\tan\varphi \tag{2}$$

in which, c is the cohesion intercept and φ is the friction angle.

2-3. Direct Shear Test

This is one of the oldest and simplest tests for measuring shear strength of soil. Figure 2 is the sketch of a typical shear box.

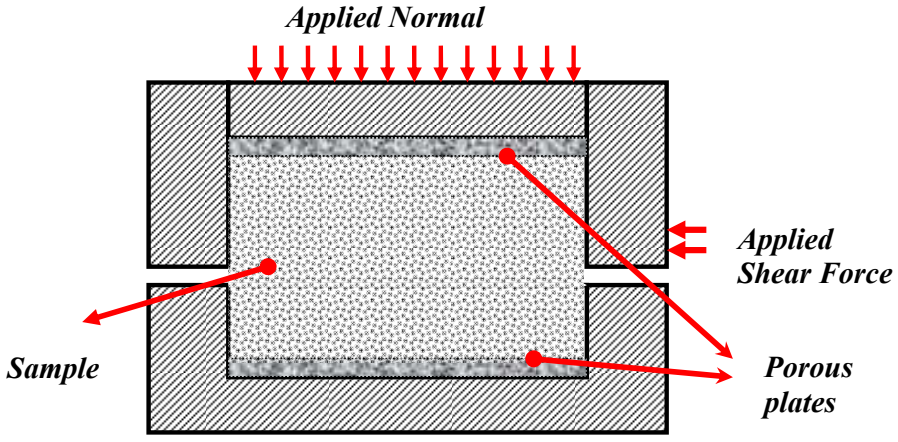

Figure 2: A sketch of a laboratory direct shear box.

A normal load is applied to the material placed in the box through the top plate, and the shear load is applied from the left (or right) side of the upper half box. During a conventional direct shear test, the amount of applied normal stress is kept a constant value while the applied shear force and normal and shear displacements are recorded for further analyses.

In order to obtain the shear strength characteristics of a soil (cohesion and internal friction angle) several direct shear tests (usually more than 2 tests) on several identical samples under different normal loads should be performed. By plotting the best linear fit through at least three points (pairs of normal stress-peak shear stress), the Mohr-Coulomb failure envelope is obtained. From this failure envelope, cohesion and friction angle are estimated. Note that in a direct shear test, the sample may not be subjected to a uniform shear distortion. Furthermore, the sample is forced to fail along a horizontal shear plane that may not be the weakest plane in the soil sample. Regardless of these problems, this test is still one of the simplest and inexpensive tests both for measuring shear characteristics of unsaturated and saturated soils, which can provide good and acceptable results. Figure 3 shows the direct shear test apparatus that was used for this study.

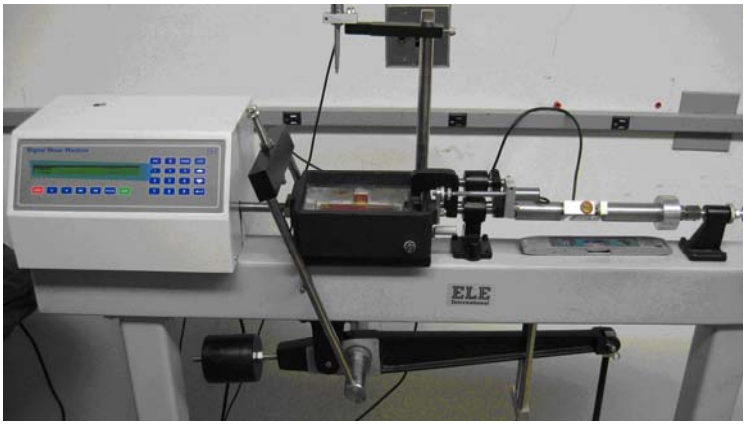

Figure 3: The digital direct shear machine at New Mexico Tech soil mechanics laboratory.

3. Sample Preparation and Shear Test Conduction

Experimental studies using a 6 cm × 6 cm shear box were conducted on the material collected from Spring Gulch rock pile that passed through No.6 sieve. The original and scalped gradation curves are shown in Figure 4. To reduce the errors associated with material variations, the rock pile material retained on sieve numbers 10, 16, 30, 40, 50, 70, 100, and passed sieve No. 100 were collected in separate containers and mixed together according to the gradation curve of Figure 4.

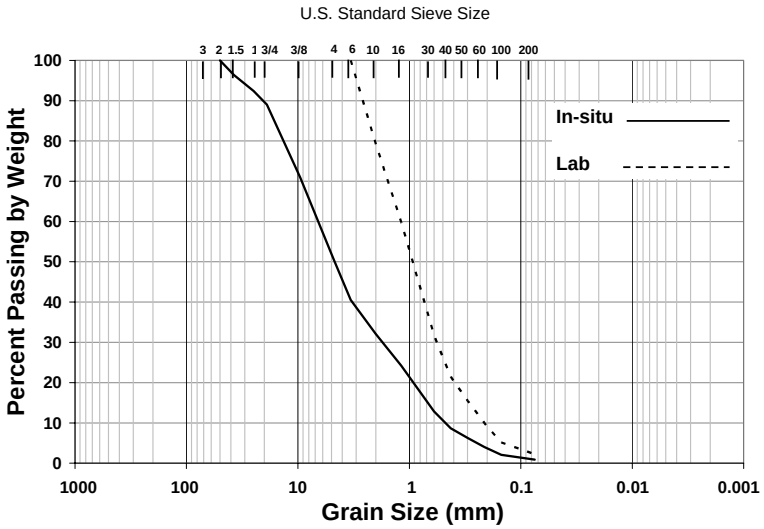

Figure 4: Gradation Curves (*in-situ* and lab) of the material used for experimental study.

The typical materials retained on different sieves and the original materials from Spring Gulch rock pile are shown in Figure 5, respectively.

(a)

(b)

Figure 5: a) The retained materials on different sieves that were mixed according to the gradation curve for sample preparation, b) The original materials from Spring Gulch rock pile.

The air dried material was mixed thoroughly with water to result in 6% water content. This water content is about the average value of the unsaturated rock pile materials that were measured in the field. Each sample is compacted in three layers in the shear box by tapping it carefully to result in a dry density of 1670 kg/m^3.

The oversize particles were simulated by using stainless steel spheres or balls having diameters of 0.66 cm, 1.28 cm, and 1.90 cm. The reason for using spherical particles was to reduce the number of parameters involved in this study; non-spherical particles can have different degrees of sphericity and angularity that add to the complexity of the problem. Also, note that in all shear tests, the dry density of the soil matrix was kept equal to 1670 kg/m^3 irrespective of the size of the oversize particle, and the compaction of the material around the steel sphere was done with special care in order to avoid inconsistency in compaction.

The oversize particles were placed along the shear plane at the center, and on the left and right sides of the shear box to investigate whether or not the location of the oversize particles modifies the shear strength. Figure 6 shows the shear box containing the steel sphere with diameter of 1.90 cm located at the center of the box. Dashed circles illustrate the location of the steel sphere when it is placed on the left and right sides of the box.

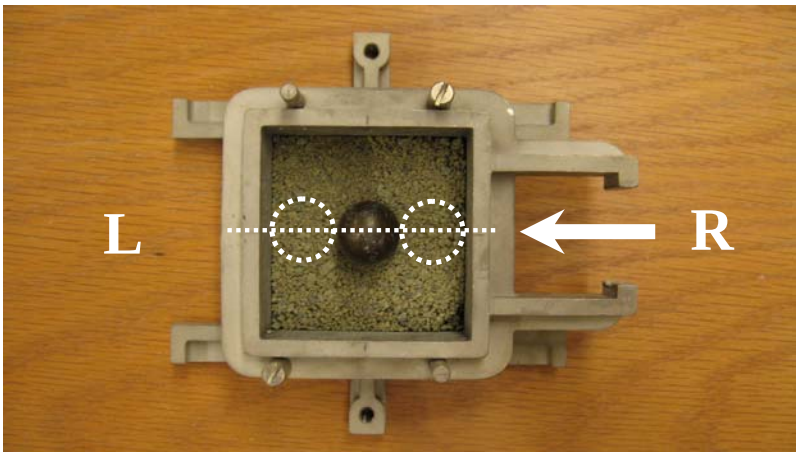

Figure 6: Shear box containing steel sphere with diameter of 1.9 cm located at the center of the box. Dashed circles represent the location of ball on the right and left sides of the box.

After preparing the sample, the shear box is placed in the automated direct shear test machine to start the test. The normal stresses used for shear testing were 20.5 kPa, 42.3 kPa, and 68.2 kPa, which are similar to those used in the *in-situ* shear testing (Boakeye, 2008). All the shear tests were conducted at a displacement rate of approximately 0.5 mm/min. Figure 7 shows a photo of the shear box in which the left and right sides of the box with respect to the location of the applied force have been depicted by letters L and R, respectively.

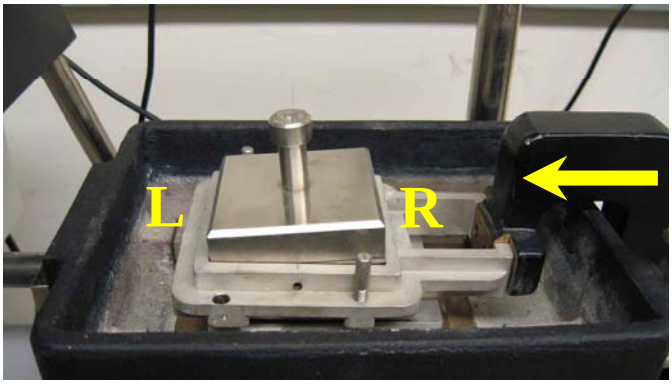

Figure 7: A photo of the shear box showing tilting of the top plate and the direction of applied shear force.

Figures 8 and 9 show different views of the sample containing the steel sphere with diameter of 1.90 cm located at the middle of the box after performing the test.

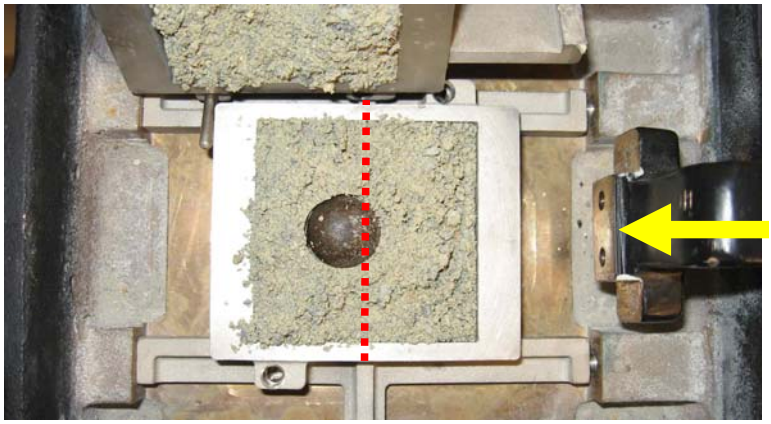

Figure 8: Top view of the shear box containing steel sphere of 1.90 cm diameter located at the middle of the box after completing the shear test.

Figure 9: Side view of the shear box containing the steel sphere of 1.90 cm in diameter after completing the shear test.

From Figure 9, it is clear that the soil material is compacted and accumulated in front of the steel sphere, which results in more resistance against the ball movement. In the next chapter, it is observed that the computer model also shows a similar material behavior.

4. Direct Shear Test Results

In total, 68 direct shear tests were performed. To assure the consistency and repeatability of the shear test results, normally more than one test was performed for a fixed ball size, ball location, and applied normal stress. All the results of the shear tests are summarized in Table 1.

Table 1: The results of laboratory direct shear tests.

Ball Diameter (cm)	*Ball Location*	*Normal Stress (kPa)*	*Test Number*	*Number of Tests*	*Peak Shear Stress (kPa)*
1.90	Left	20.5	1	3	39.2
			2		36.6
			3		35.1
		42.3	4	2	70.2
			5		65.8
		68.2	6	2	89.2
			7		90.7
	Middle	20.5	8	2	30
			9		30
		42.3	10	2	50.2
			11		51.2
		68.2	12	3	81.9
			13		74.6
			14		83.4
	Right	20.5	15	3	30.7
			16		30.7
			17		32.2
		42.3	18	3	54.1
			19		54.1
			20		51.2
		68.2	21	3	77.5
			22		80.9
			23		79
1.28	Left	20.5	24	3	29.3
			25		31.9
			26		30.7
		42.3	27	2	47.2
			28		48.3
		68.2	29	2	72.8
			30		77.2
	Middle	20.5	31	2	30.7
			32		26.3
		42.3	33	2	51.2
			34		54.6
		68.2	35	2	74.6
			36		72.8
	Right	20.5	37	2	29.3
			38		25.6
		42.3	39	3	45.8
			40		50.2
			41		43.9
		68.2	42	3	70.2
			43		73.1
			44		73.6

Ball Diameter (cm)	*Ball Location*	*Normal Stress (kPa)*	*Test Number*	*Number of Tests*	*Peak Shear Stress (kPa)*
0.66	Left	20.5	45	2	24.9
			46		27.5
		42.3	47	2	45.3
			48		43.9
		68.2	49	2	70.2
			50		68.8
	Middle	20.5	51	3	25.3
			52		26.3
			53		27.8
		42.3	54	2	49.7
			55		52.7
		68.2	56	2	66.6
			57		68.8
	Right	20.5	58	1	24.9
		42.3	59	1	43.9
		68.2	60	1	67.3
No Ball	N/A	20.5	61	3	27.8
			62		29.3
			63		29.3
		42.3	64	2	52.7
			65		48.3
		68.2	66	3	68.8
			67		73.1
			68		70.2

The average shear stress-shear displacement curves for the shear tests with the normal stress of 68.2 kPa are shown in Figures 10 through 12. The average shear stress-shear displacement curves for the shear tests at the normal stresses of 42.3 kPa and 20.5 kPa are also in appendix A.

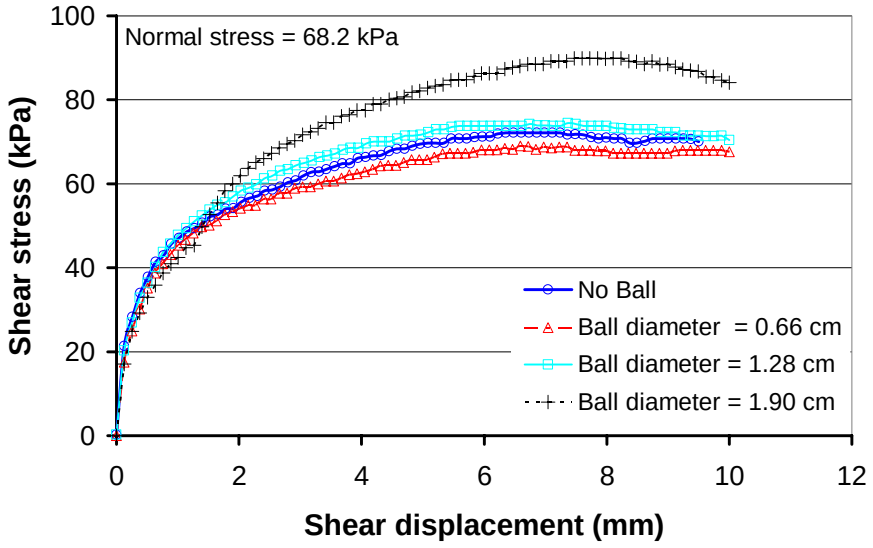

Figure 10: Shear stress vs. shear displacement for the ball located on the left side of the box.

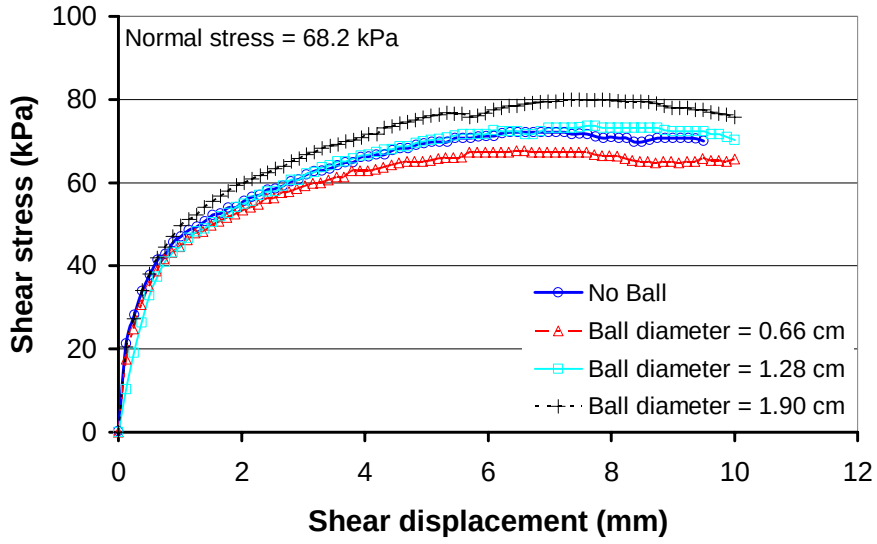

Figure 11: Shear stress vs. shear displacement for the ball located at the center of the box.

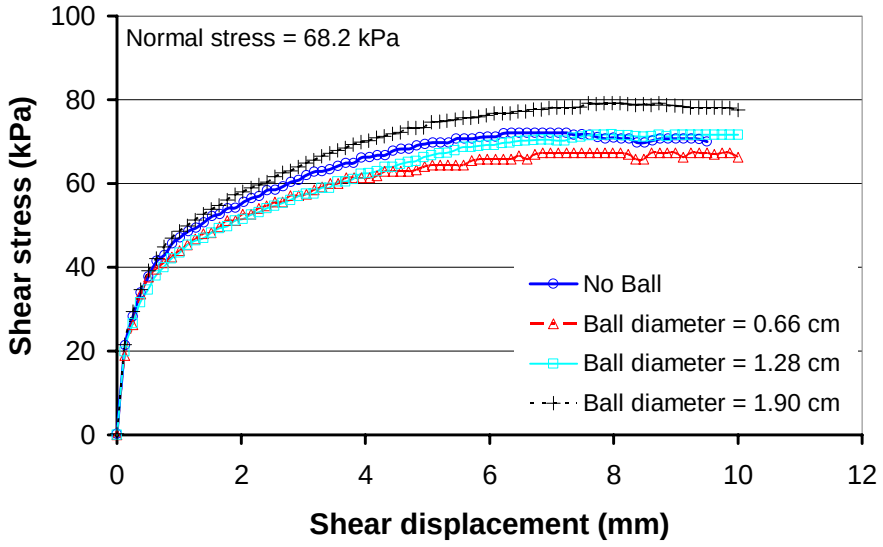

Figure 12: Shear stress vs. shear displacement for the ball located on the right side of the box.

Figures 13 to 15 show the Mohr-Coulomb failure envelopes of the laboratory samples. Each envelop is a regression line passing through all the points of shear test results with the same ball size and ball location.

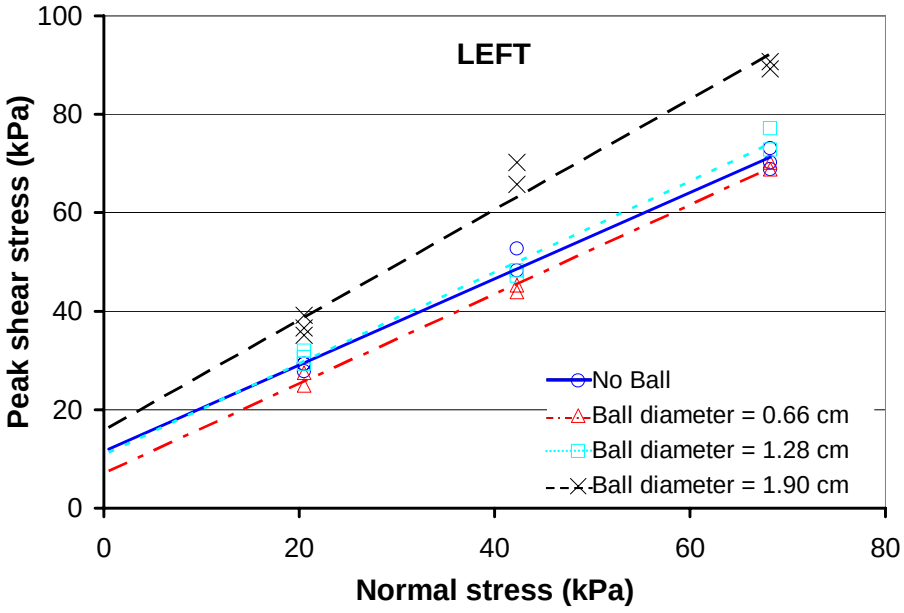

Figure 13: Mohr-Coulomb failure envelopes for the samples with the steel ball located on the left side of the shear box.

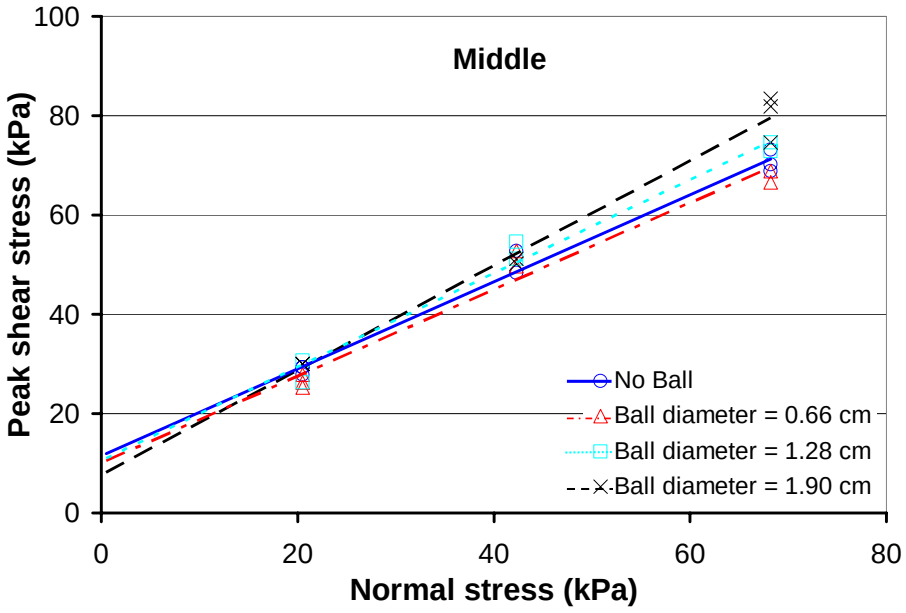

Figure 14: Mohr-Coulomb failure envelopes for the samples with the steel ball located at the center of the shear box.

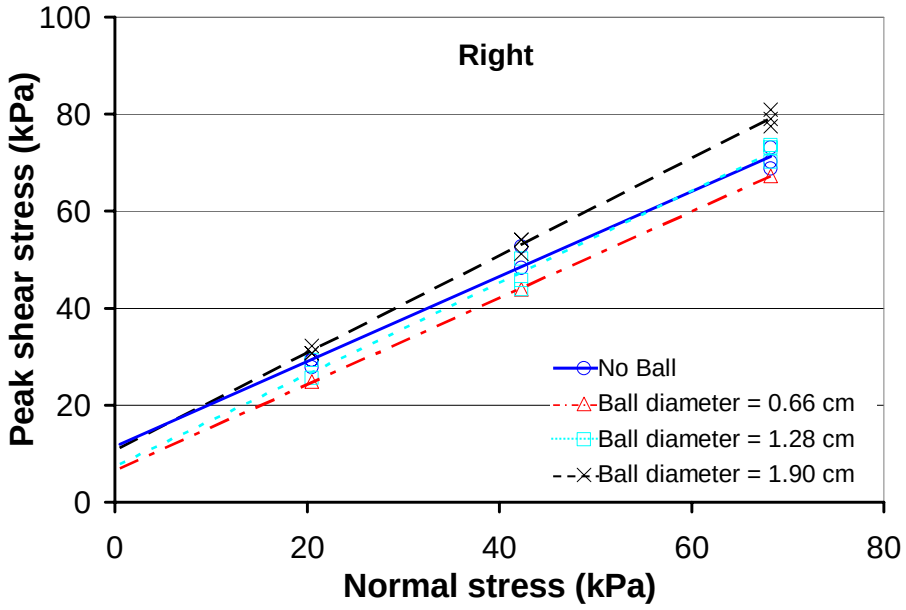

Figure 15: Mohr-Coulomb failure envelopes for the samples with the ball located on the right side of the shear box.

Figures 10 to 15 suggest that the presence of the oversize particle changes the shear strength of the material, and that this effect is more pronounced when the largest oversize particle (1.90 cm in diameter) is used. To investigate the dilatational behavior of the material, the average normal displacements at the center of top plate versus the shear displacement for the normal stress of 68.2 kPa are shown in Figures 16 through 18. Except for the largest ball, the dilatational behavior of the material remained almost unchanged. As expected, the test with largest ball shows more dilatation, indicating that more energy is needed to shear the material that is consistent with the higher peak shear stresses in Figures 10 through 12. Note that in Figures 16 through 18 the points corresponding to the peak shear stresses are shown with larger symbols, suggesting that a greater shear displacement corresponding to the peak shear stress is observed for the shear tests with the two largest balls. The average normal displacements at the center of top plate versus the shear displacement for the normal stress of 42.3 and 20.5 kPa are provided in appendix A.

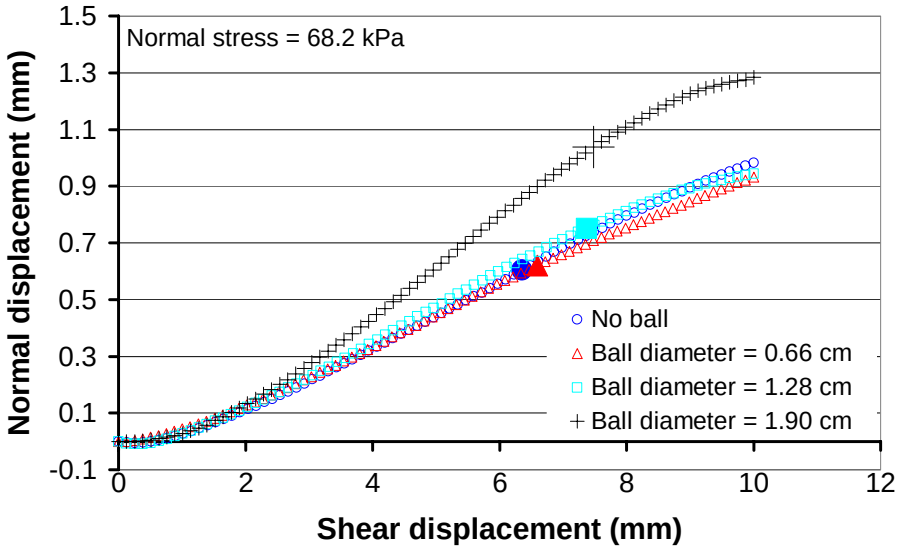

Figure 16: Normal displacement vs. shear displacement for the samples with the steel ball located on the left side of the box.

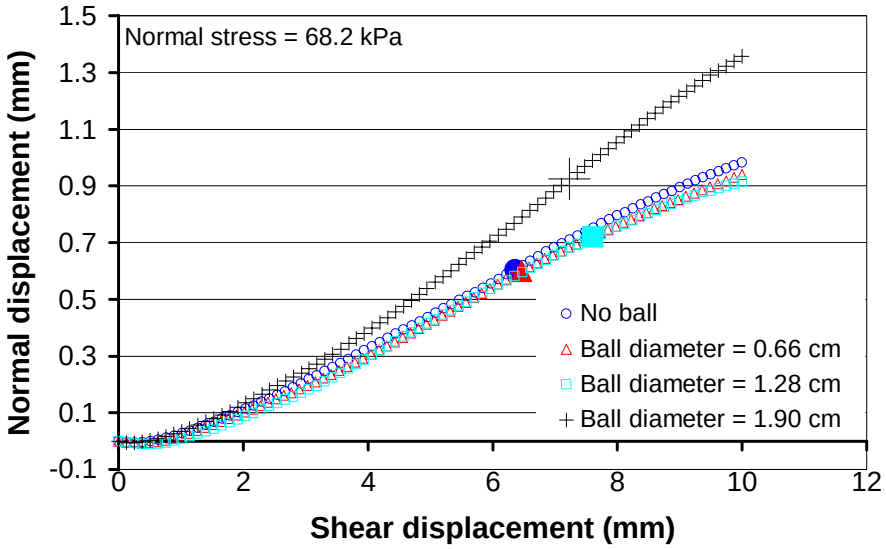

Figure 17: Normal displacement vs. shear displacement for the samples with the steel ball located at the center of the box.

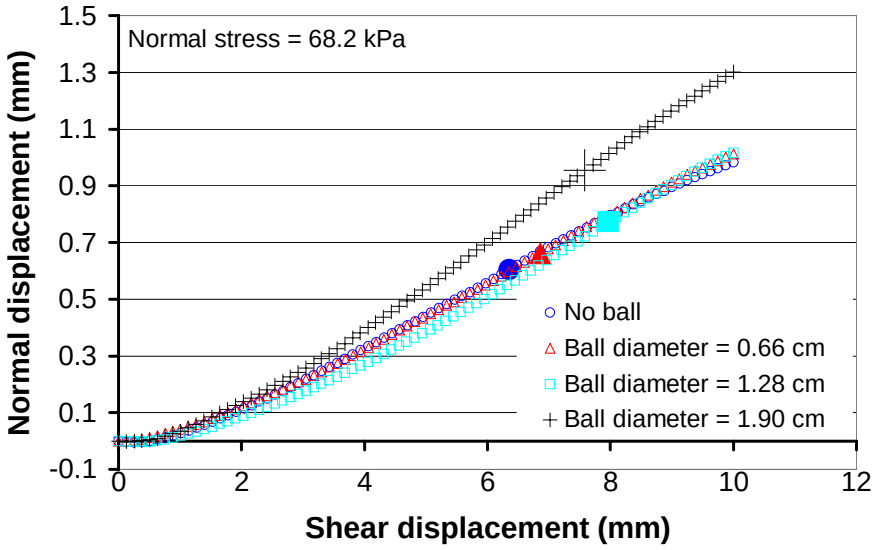

Figure 18: Normal displacement vs. shear displacement for the samples with the steel ball located on the right side of the box.

The friction angles (φ), dilation angles (ψ), and cohesion intercepts (c) from direct shear tests are reported in Table 2. The dilation angles corresponding to the

peak shear stresses and a normal stress of 68.2 kPa were obtained from Figures 16 through 18 using the following equation:

$$\tan(\psi) = \frac{d\varepsilon_{yy}}{d\gamma_{xy}} = \frac{dv}{du} \tag{3}$$

where ε_{yy} and γ_{xy} are normal and shear strains, and v and u are vertical (normal) and shear displacements, respectively. Note that this equation is valid only if the shear plane is assumed to be a zero extension line.

Table 2: The measured friction angles, dilation angles, and cohesions in the direct shear tests.

Ball diameter (cm)	*Location of the ball*	*φ (Degree)*	*Dilation angle (Degree) (Normal stress 68.2 kPa)*	*c (kPa)*
D = 1.90	Left	48.2	9.0	15.8
	Middle	46.5	10.1	7.6
	Right	45.1	8.7	10.6
D = 1.28	Left	42.8	5.9	10.8
	Middle	43.3	5.1	10.5
	Right	43.4	7.4	7.4
D = 0.66	Left	42.3	6.1	7.1
	Middle	41.1	6.8	10.1
	Right	42.8	6.9	8.9
No Ball	N/A	41.2	7.1	11.5

As expected, the data in Table 2 show that in general the dilation angle increases with increase in friction angle. The friction angles, dilation angles, and cohesions of the material with and without the oversize ball shown in Table 2 indicate how the shear strength and deformational characteristics of the material are affected by the ball size.

In Figure 19, the variation of friction angle as a function of normalized ball diameter with respect to box width is shown. It is clear that the friction angle increases with increase in the ball diameter. The maximum increase in the friction

angle is for the test with the largest ball located on the left side of the box that shows a friction angle of 48.2° compared to the no ball situation whose friction angle is 41.2°. The friction angle of 48.2° is higher than those of 46.5° and 45.1° obtained for the situations where the largest ball is accommodated in the middle and on the right side of the box, respectively. Laboratory observations suggest that depending on the location of the oversize ball in the shear box, different kinematical constraints in the box deformation affect the shear strength of the material. For example, even though the final vertical displacement of the center of top plate was almost the same in all the three tests shown in Figures 16 through 18, the tilting of top plate (Figure 7) was slightly different depending on the location of the oversize ball. Note also that tilting of the top plate causes a non-uniform distribution of soil density and normal stress within the deformed sample and that can be another reason for sensitivity of the shear tests results with the largest ball to the ball location.

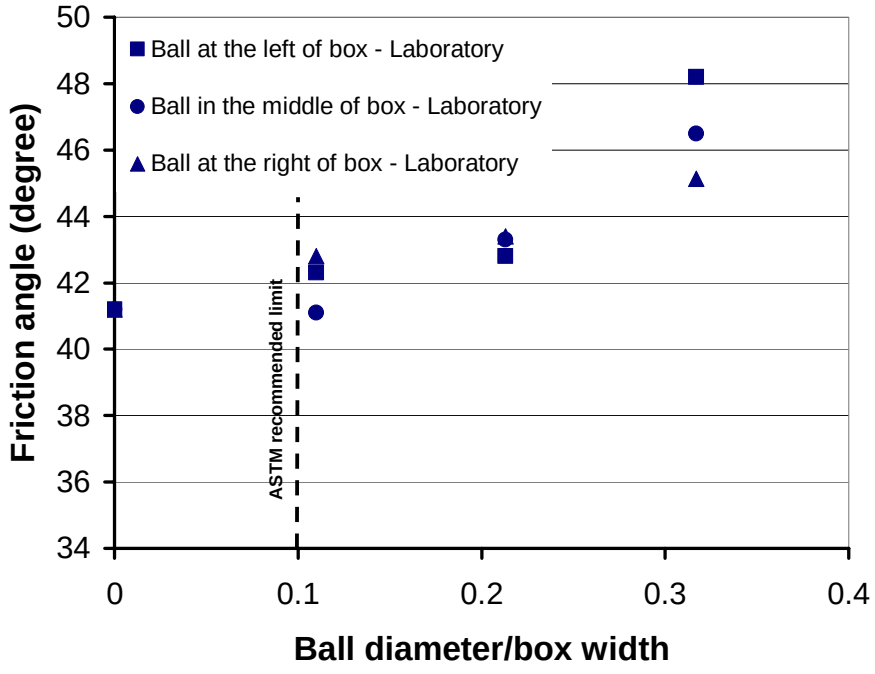

Figure 19: Friction angle vs. normalized ball diameter. The allowable maximum particle size/box width recommended by ASTM is shown with the dashed line.

It is important to realize that the increase in friction angle due to presence of oversize ball is only a couple of degrees even when the normalized ball diameter is equal to 20%. This indicates that the recommendation regarding the maximum allowable particle size in a direct shear tests by ASTM (maximum particle size / box width < 0.1) can be somewhat relaxed, at least for the rock pile material in this study and the given range of low normal stresses.

Figure 20 illustrates the cohesion intercept versus the normalized ball diameter. Except for the largest ball located on the left side of the box, the cohesion reduced due to presence of oversize particle. Depending on the location of the ball and its size, the decrease in cohesion intercept could be 10 to 40% with an average of 15%. Nevertheless, cohesion in general is more sensitive to soil remoulding compared to friction angle, and its measurement in the lab might be questionable.

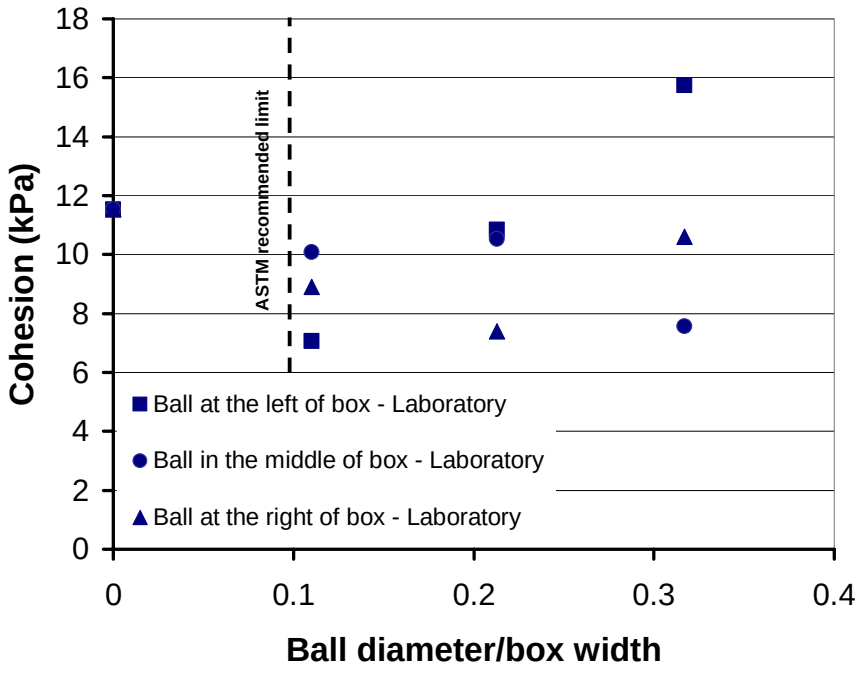

Figure 20: Cohesion vs. normalized ball diameter. The allowable maximum particle size/box width recommended by ASTM is shown with the dashed line.

5. Conclusion

To study the effect of oversize particles on the shear strength of soil, several direct shear tests with samples 6 cm × 6 cm in size were conducted on the Questa mine rock pile materials. To simulate the oversize particles, spherical balls made of stainless steel with different diameters were placed along the shear plane. The results of direct shear tests suggest that in general both the friction angle and dilation angle increase due to the presence of the oversize particle, even though the effect of an oversize particle is much more pronounced on the friction angle compared to that on the dilation angle. The recommendation made by ASTM regarding the allowable maximum particle size seems to be too conservative for the case studied, i.e., for the low normal stress used and the rock pile material investigated. Instead of a limit of 0.1 for the ratio of maximum particle size to box width, a ratio of 0.2 can be applied with only minimal increase in friction angle (about 2 degrees). The results of this study show also that cohesion is normally underestimated if oversize particles are present in the shear box.

CHAPTER 3
Numerical Modeling of The Laboratory Shear Box

1. Introduction

Laboratory test results in the previous chapter suggest that the presence of an oversize particle can cause an increase in friction and dilation angles while in general the cohesion intercept decreases. In order to interpret the laboratory findings in more detail, numerical modeling of the laboratory direct shear tests was conducted. The computer program CA2 (Fakhimi, 1998), which is a hybrid discrete-finite element program was used for this investigation. The shear box is modeled with finite elements while the rock pile material is simulated with a discrete element system. The discrete particles motions together with the micro damage evolution are studied in this numerical model to elucidate the role of oversize particle on the shear distortion of the material. In this chapter, first the theoretical aspects of the discrete element model are briefly discussed, and then the results of numerical simulation of the shear box are reported.

2. Theory

The discrete element model (DEM) was originally introduced by Candull (1971) for the analysis of rock mechanics problems and then applied to soils by Cundall and Strack (1979). Since assemblies of discrete particles can capture the complicated behavior of granular material, which arises as an emergent property of the assembly, it appears that the discrete element modeling of rock and soil is more appropriate compared to the continuum models.

In the discrete element method, particles interact like a dynamic process, and their interaction develops the internal or contact forces. The contact forces and displacement of the particles are obtained by recording the movement of each particle. The source of movement of particles can result from the movement of a specific wall or particle. The propagation speed depends on the defined velocity for each timestep in addition to physical properties of the model. Hence, if we desire to solve a static problem, the applied velocities must be very small, in the way that the dynamic solution of DEM can provide the desired static solution.

Computations in DEM apply the force-displacement law and Newton's second law for each contact. For obtaining the contact forces created from relative motion at each contact, the force-displacement law is used, while for determining the motion of each particle provided by the contact and body forces, the Newton's second law is used. The calculation cycle in CA2 is a timestep in which the law of motion to each particle, wall positions, and the force-displacement law to each contact are updated. The procedure that the program follows in each time step is as follows:

First, the position of particles and walls at the contacts are updated. Then based on the relative motion between two entities at the contact point and the contact

constitutive model, the force-displacement law is used for each contact to compute the new contact forces. Finally, for computing the new velocity vector and position of each particle, the law of motion is applied. Figure 21 shows a computational cycle in CA2 program.

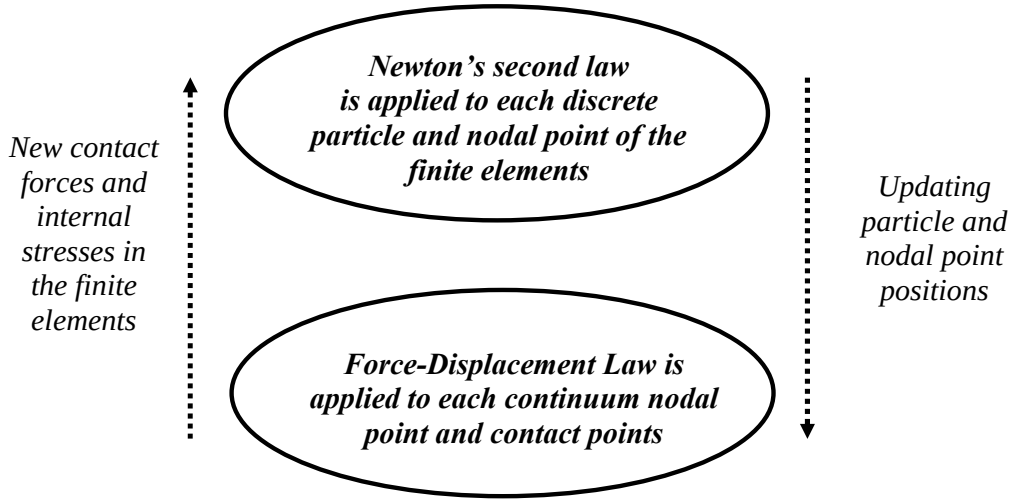

Figure 21: A calculation cycle in CA2 program.

2-1. Force – Displacement law

The formulation of the discrete element model in this chapter follows the work reported in Itasca (1999). As mentioned, the force-displacement law is the relation between the relative displacement between two entities at a contact and the contact force acting on the entities. Figure 22 shows a cylinder-cylinder contact in a two-dimensional space.

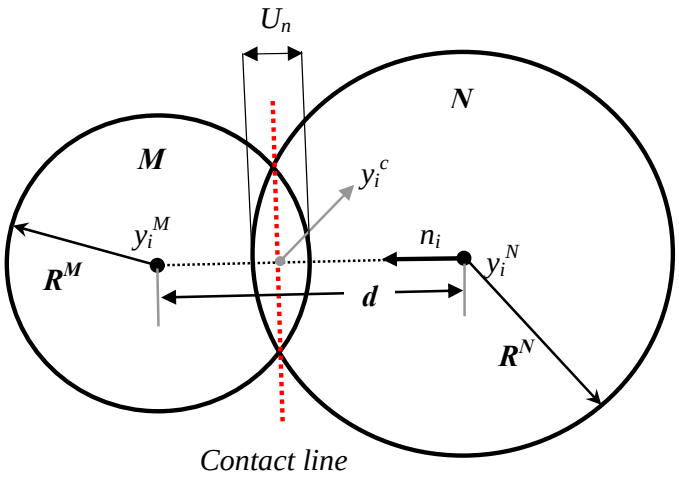

Figure 22: Illustration of interaction between two cylinders.

Here, n_i represents the unit normal vector between two cylinders that defines the contact line. The vector n_i is obtained through the following equation:

$$n_i = \frac{y_i^M - y_i^N}{d} \tag{4}$$

where y_i^M and y_i^N represent the position vectors of the center of cylinders M and N, and d is the distance between the cylinder centers. The distance between the cylinder centers can be computed by the following equation:

$$d = \sqrt{(y_1^M - y_1^N)^2 + (y_2^M - y_2^N)^2} \tag{5}$$

By considering the known radii of cylinders, R^M and R^N, in addition to the distance between the cylinders' centers, we can calculate U_n, the overlap of cylinders M and N, using the following equation (for cylinder-cylinder contact):

$$U_n = R^M + R^N - d \tag{6}$$

The coordinate of the contact point, y_i^c, is given by:

$$y_i^c = y_i^M - (R^M - \frac{1}{2}U_n).n_i \tag{7}$$

For cylinder-wall contact, n_i is directed along the line defining the shortest distance, d, between the cylinder center and the wall. Figure 23 shows the contact between the cylinder and wall in addition to the notations used to describe cylinder-wall contact.

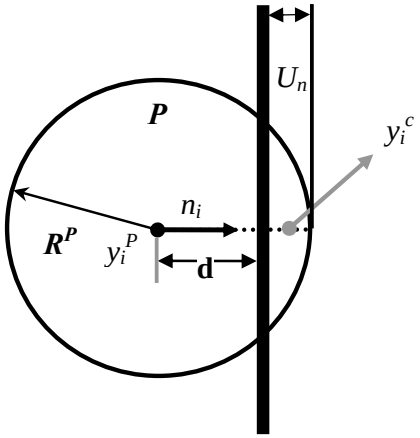

Figure 23: Illustration of the cylinder-wall contact.

Using the same logic used for cylinder-cylinder contact, we can calculate the U_n, the relative contact displacement in the normal direction, for the cylinder-wall contact as follows:

$$U_n = R^P - d \quad \text{(Cylinder-Wall Contact)} \tag{8}$$

And the coordinate of cylinder-wall contact point is:

$$y_i^c = y_i^P + (R^P - \frac{1}{2}U_n).n_i \quad \text{(Cylinder-Wall Contact)} \tag{9}$$

The contact force vector (F_i) representing the action of cylinder M on cylinder N for cylinder-cylinder contact and representing the action of the cylinder on the wall for cylinder-wall contact can be decomposed into the normal force F_i^n and shear force F_i^s with respect to the contact plane:

$$F_i = F_i^n + F_i^s \tag{10}$$

The contact velocity V_i defined as the relative velocity of cylinder M to cylinder N at the contact point for cylinder-cylinder contact, or for the cylinder-wall contact, it can be defined as the relative velocity of the wall to cylinder at the contact point. For obtaining the relative velocity at the contact point, the following equations are used:

$$V_i = (\frac{\partial y_i^c}{\partial t})_\psi - (\frac{\partial y_i^c}{\partial t})_\xi$$

$$= (\frac{\partial y_i^\psi}{\partial t} + e_{i3k}.\omega_3^\psi (y_k^c - y_k^\psi)) - (\frac{\partial y_i^\xi}{\partial t} + e_{i3k}.\omega_3^\xi (y_k^c - y_k^\xi)) \quad (11)$$

where ψ and ξ are the entities that can be cylinder-cylinder or cylinder-wall, ω_3^ψ and $\frac{\partial y_i^\psi}{\partial t}$ are the rotational and translational velocity, respectively, and e_{i3k} is the permutation symbol. The contact velocity can be decomposed into normal and shear components, which are donated by V_i^n and V_i^s respectively. Hence, the relative contact velocity can be written as follows:

$$V_i = V_i^n + V_i^s \quad (12)$$

The incremental shear displacement component over a timestep of Δt is obtained by:

$$\Delta U_i^S = V_i^S . \Delta t \quad (13)$$

2-2. Contact-Stiffness Models

The contact forces and relative displacements in the normal and shear direction area related by the contact stiffnesses:

$$F^n = k^n U^n \quad (14)$$

Where F^n is the contact normal force, U^n is the overlap of the cylinders, and k^n is the normal contact stiffness. Equation (14) is used in CA2 during the

discrete sample preparation while for the deviatoric loading of the sample, an incremental law is used:

$$\Delta F^n = k^n \Delta U^n \tag{15}$$

where ΔF^n and ΔU^n are the increments of contact normal load and displacement, respectively. A similar equation is used to obtain the increment of contact shear force (ΔF^S) from the increment of contact shear displacement (ΔU^n) using the contact shear stiffness (k^S):

$$\Delta F^S = -k^S \Delta U^S \tag{16}$$

If the contact shear or tensile normal force between two particles exceeds the shear and normal bonds, the contact breaks. For a failed contact, the Coulomb's law governs the maximum shear force that can be carried by the contact:

$$F_{s(\max)} = \mu \left| F_n \right| \tag{17}$$

in which μ is the friction coefficient.

3. Numerical Modeling of Laboratory Shear Box

Figure 24 shows a sketch of the numerical model of the shear box. The box is made of five pieces shown with letters A, B, C, D, and E. All of these regions are discretized into finite elements that for the sake of clarity are not shown in the figure. The top half of the box has been divided into four pieces (A, B, C, and D). The top plate C is in contact with the vertical side B of the box through the interface B2B4-C1C3. No interface was defined along A1A3-C2C4 to allow free rotation of the top plate. The sides of each interface in CA2 program interact with each other through normal and shear springs. The interface B2B4-C1C3 between the top plate and box

side B has no cohesion and friction to provide additional freedom to movement and rotation of the top plate, and to help to fully transfer the applied normal stress to the simulated soil sample. The A1A2-E5E6 and B1B2-E1E2 are also defined as interfaces with no friction and cohesion to prevent interpenetration of the side boundaries of the shear box. The region D (D1D3D4D2) in Figure 24 is used to provide the mechanical connection of the left and right sides B and A of the box and to help, approximately, simulate the three dimensional effects. This region (D) is connected to both vertical sides, A and B, through interfaces B2B4-D1D3 and A1A3-D2D4, respectively. These interfaces are assigned with high tensile and shear strengths to prevent disintegration of the box due to the applied stresses.

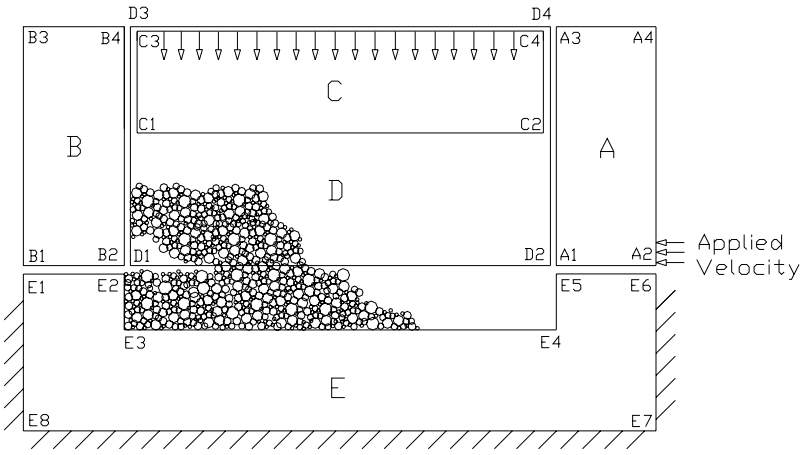

Figure 24: A Sketch of the shear box used for the numerical simulation.

Internal surfaces of the box are defined as "walls" in the CA2 program to allow interaction between the discrete elements and finite elements. Each discrete element in CA2 is a circular cylinder. The cylinder-cylinder and cylinder-wall interactions are modeled by normal and shear springs, normal and shear bonds, and a friction coefficient. Therefore, the micromechanical constants for cylinder-cylinder or cylinder-wall interactions are the normal and shear spring constants (k_n and k_s), the

normal and shear bonds (n_b and s_b), and the friction coefficient (μ). This simple contact bond model (Itasca, 1999) behaves elastically under the applied stresses until the tensile normal force or shear force at a contact point exceeds the normal or shear bond leading to tensile or shear failure at that contact point. A failed contact point loses its bond permanently but still it can carry shear forces through a Coulomb law using the friction coefficient μ if it is subjected to a compressive load.

In addition to the above micro-parameters, the radius of cylinders and the genesis pressure must be specified. The genesis pressure is the applied compressive stress to the discrete system during the sample preparation when there is no friction or contact bond between the particles to allow the particles to move easily and fill in the gaps between the particles. The genesis pressure during sample preparation causes slight overlap of the cylinders. This overlap helps to simulate more realistic friction angle of geomaterials as reported by Fakhimi (2004).

Based on laboratory direct shear tests on the Spring Gulch material, an average friction angle (φ) of 41.2° and an average cohesion of 11.5 kPa were obtained. The elastic modulus and Poisson's ratio were assumed as E = 16.8 MPa and ν = 0.2, respectively. These macroscopic properties together with the cylinders radii (R) of 0.3 to 0.6 mm were used to obtain the corresponding micro-properties (k_n, k_s, n_b, s_b, μ, and σ_0) through a calibration procedure (Fakhimi and Villegas, 2007). The following micro-properties were obtained:

k_n = 33.1 MPa, k_s = 7.6 MPa, n_b = 18.5 N/m, s_b = 18.5 N/m, μ = 1.0, and σ_0/k_n=0.041. These micro-properties together with cylinder-wall contact properties of k_n = 10.0 GPa, k_s = 10.0 GPa, μ = 0.5, and n_b = s_b = 0.0 were used in simulations of a direct shear test and a biaxial test without any oversize cylinder. These simulations

confirmed that the selected micro-properties were in fact able to reproduce the correct macro-properties.

Note that the diameters of the cylinders were selected based on the particle size D_{50} of 0.9 mm in Figure 4; the cylinders' diameters were allowed to have a random uniform distribution between D_{50}-0.3 mm and D_{50}+0.3 mm. Therefore, the cylinders radii of the cylinders ranged from 0.6 mm to 1.2 mm in the numerical model. The total number of the discrete cylinders in the shear test simulation with no oversize cylinder was (2217). Similar to the physical test situations, the oversize cylinders 0.66 cm, 1.28 cm, and 1.90 cm in diameter were placed along the shear plane. The applied normal stresses were the same as in the laboratory tests. Figure 24 shows the applied normal stress at the top surface of the top plate and the fixed external boundary of the bottom half of the box in the numerical model. The shear force was induced in the system by applying a constant velocity of 4.5×10^{-9} m/numerical cycle to the bottom part of side A2A4 of top half box that is shown with arrows in Figure 24. The applied velocity was small enough to result in a quasi-static solution of the problem.

4. Numerical Results

The first step in numerical modeling of the shear box is sample preparation to provide the required normalized genesis pressure of $\sigma_0/k_n=0.041$. At this stage, the vertical and horizontal external boundaries of the box are fixed in the x and y directions, respectively. Following the sample preparation, the initial stresses, the contact forces, and the velocities are initialized to zero and the normal and shear bonds and friction are introduced to the cylinders. The system is then allowed to reach equilibrium under the weight of the simulated soil sample. In this situation, only the

bottom half of the shear box is fixed at its external surfaces in x and y directions. The normal stress is then applied to the top plate and the problem is solved to achieve equilibrium. A shear test starts by applying a constant horizontal velocity to the bottom edge of the right side of top half box as shown in Figure 24. The applied velocity was 4.5×10^{-9} m/numerical cycle to assure a quasi-static situation during the numerical shear tests. Note that the placement of the oversize particle in the shear box was performed by excavating the material and then replacing the excavated cylinders with the oversize particle. This procedure helped to preserve the original matrix and the cylinders distribution in the numerical sample.

The shear stresses versus shear displacements from the numerical shear tests for the situations that the oversize cylinder is placed on the left, center, and right sides of the box with the normal stress of 68.2 kPa are shown in Figures 25, 26, and 27. Each shear stress-shear displacement curve like the experimental one shows an initial linear behavior that is followed with the plastic deformation. From Figures 25, 26, and 27, it is clear that with the placement of the larger oversize cylinders in the shear box, the peak shear stress increases that is consistent with the experimental findings. Complementary results of numerical model for normal stresses of 42.3 and 20.5 kPa are provided in appendix B.

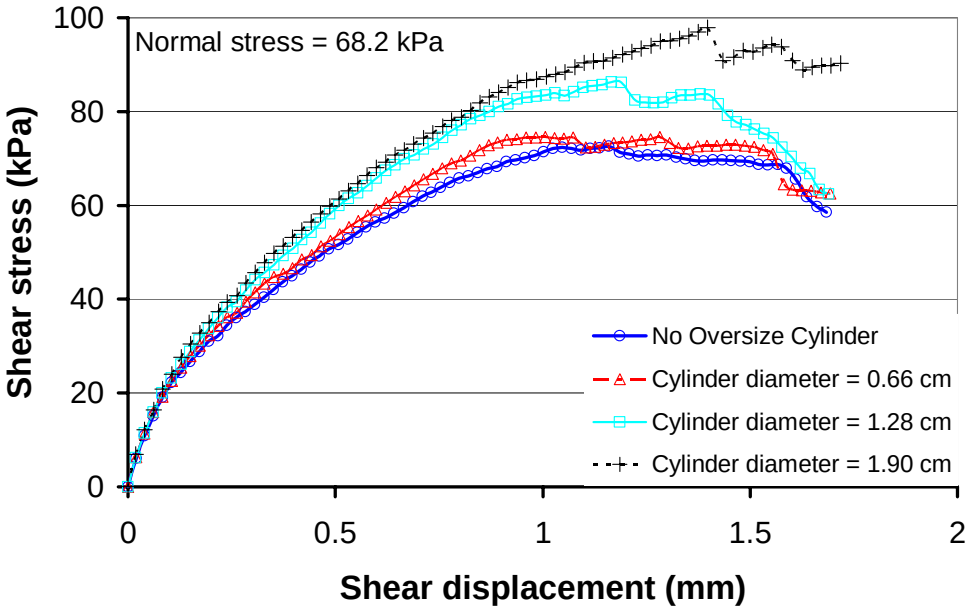

Figure 25: Shear stress vs. shear displacement of the numerical shear tests with the applied normal stress of 68.2 kPa for the oversize cylinder placed on the left side of the box.

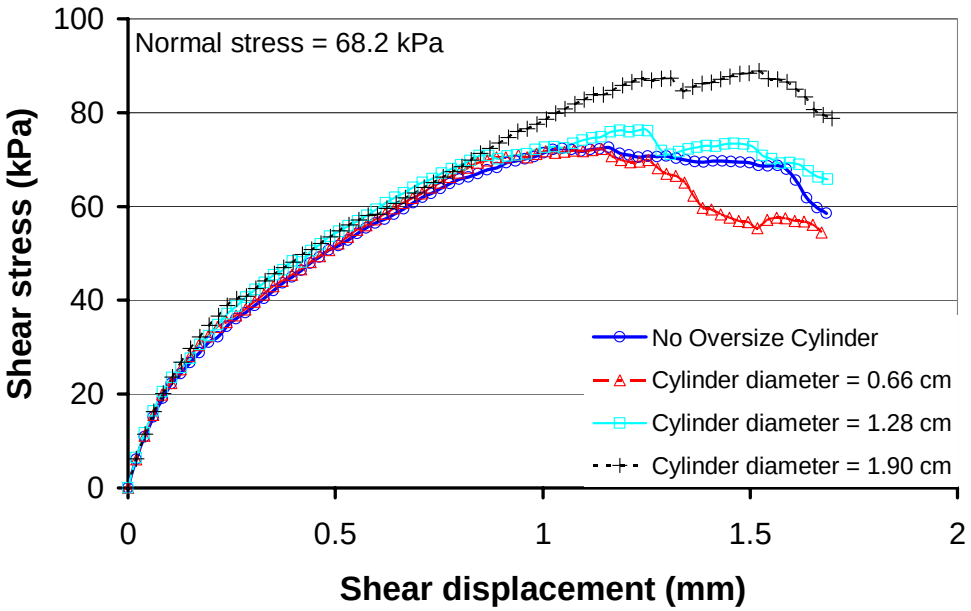

Figure 26: Shear stress vs. shear displacement of the numerical shear tests with the applied normal stress of 68.2 kPa for the oversize cylinder placed at the center of the box.

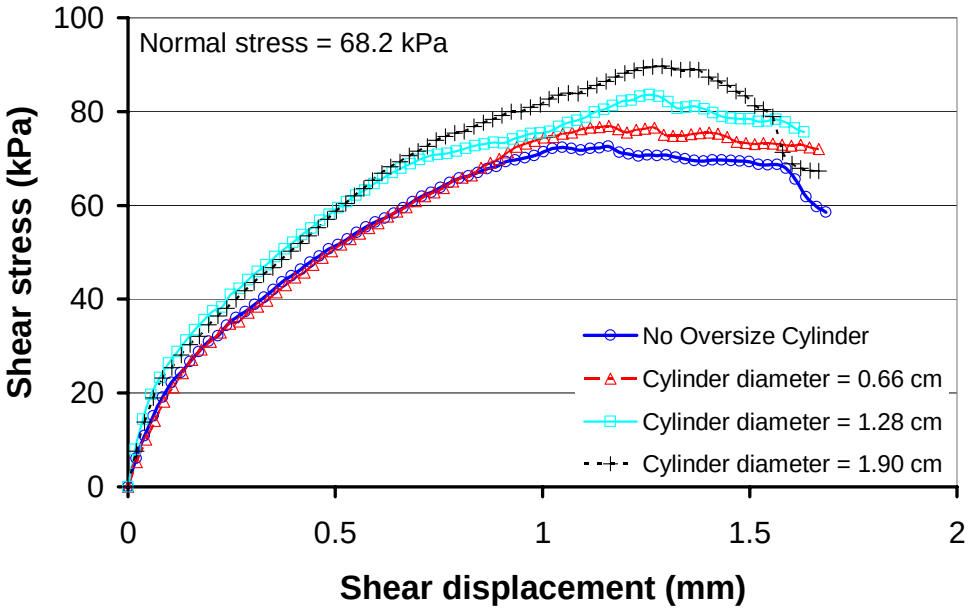

Figure 27: Shear stress vs. shear displacement of the numerical shear tests with the applied normal stress of 68.2 kPa for the oversize cylinder placed on the right side of the box.

5. Discussion of the Experimental and Numerical Results

The shear stress-shear displacement behavior of the experimental samples in Figures 10, 11, and 12 (from chapter 2) and those of numerical modeling in Figures 25, 26, and 27 show some overall similarities, but there are a few differences as well that need to be discussed. The laboratory tests show almost a perfect plastic behavior with no or small softening at the given dry density and the range of applied low normal stresses. The reason for this behavior could be due to the fact that part of the cohesion in the unsaturated rock pile samples is due to the matric suction that is not easily lost by shear deformation. On the other hand, the numerical tests show more pronounced post peak softening behavior. Furthermore, shear displacements corresponding to the peak shear stresses in the numerical tests are smaller than those in the experimental tests. Both these features in the numerical model are due to the

brittle behavior of the contact bond model used for simulation of the rock pile material. A contact bond model loses its strength immediately once the applied shear or normal contact force exceeds the shear or normal bond that is not realistic for these rock pile materials. A softening contact bond model (Fakhimi et al., 2005) allows a gradual loss of the contact bond that should help reduce the discrepancy between the physical and numerical shear behaviors. Nevertheless, the numerical and experimental tests show similar trends in the shear strength change of the material due to the presence of oversize cylinder that is discussed in this section.

To investigate the role of oversize particle, the development of micro-cracks and the displacement field of the cylinders were studied in the numerical model. A micro-crack in CA2 is a line perpendicular to the line connecting the centers of two cylinders with broken bond. The micro-cracks in the numerical simulations, with the normal stress of 68.2 kPa after 3.5 mm of shear displacement for the shear tests without the cylinder and with the largest cylinder (1.90 cm in diameter) placed on the left, center, and right sides of the box, are shown in Figure 28. Tensile cracks are shown in red while the shear cracks are in blue. From Figures 28a, 28b, 28c, and 28d, it is evident that the shear band and crack pattern are affected by the presence of oversize particle. In particular, the damaged zone is more extensive when the oversize cylinder is placed on the left side of the box.

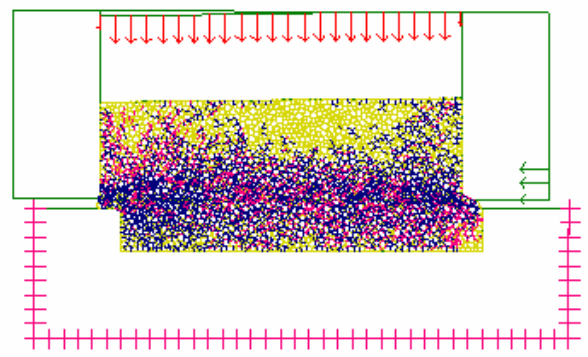

(a)

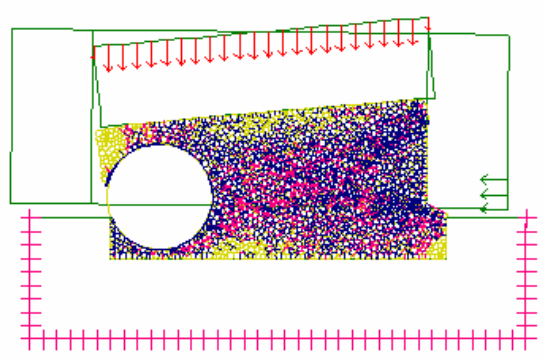

(b)

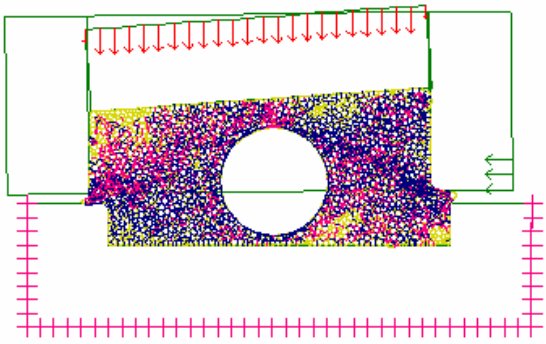

(c)

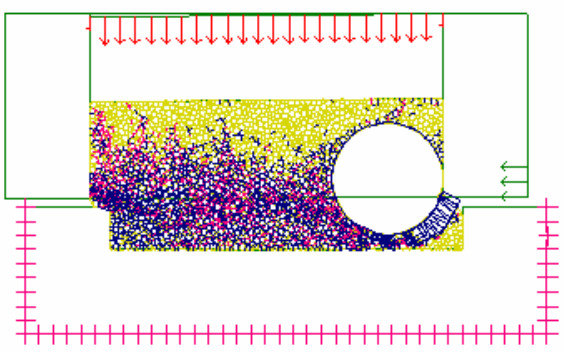

(d)

Figure 28: Micro-cracks in the numerical samples with the applied normal stress of 68.2 KPa after 3.5 mm shear displacement for the sample a) without the oversize cylinder, b) with the largest oversize cylinder on the left side of the box, c) with the largest oversize cylinder placed at the center of the box, and d) with the largest oversize cylinder placed on the right side of the box. Tensile and shear cracks are in red and blue, respectively.

The deformed shapes of the numerical samples with the applied normal stress of 68.2 kPa after 3.5 mm shear displacement, for the sample without the oversize cylinder and for the samples with the largest oversize cylinder placed on the left side, at the center, and on the right side of the box are shown in Figure 29. The dark and light bands in the samples were initially vertical before any shear displacement was applied. Therefore, the deformed bands in Figures 29a to 29d illustrate the concentration of shear deformation along the shear band.

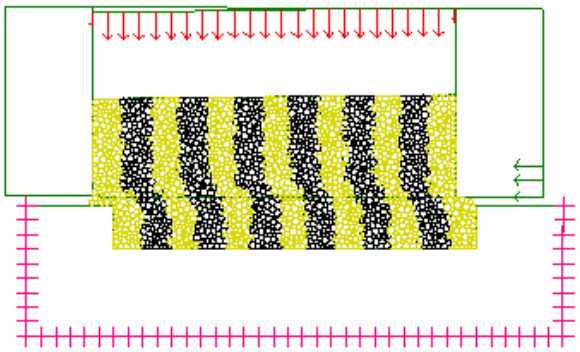

(a)

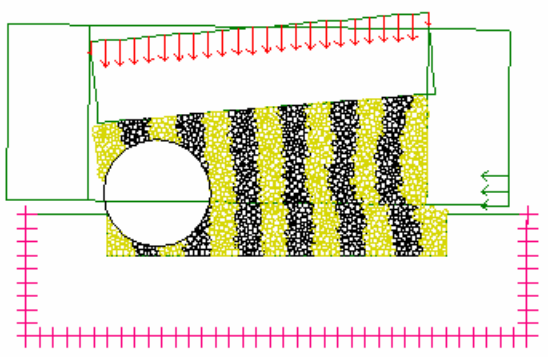

(b)

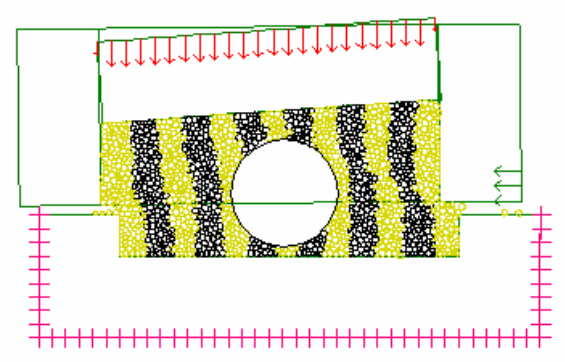

(c)

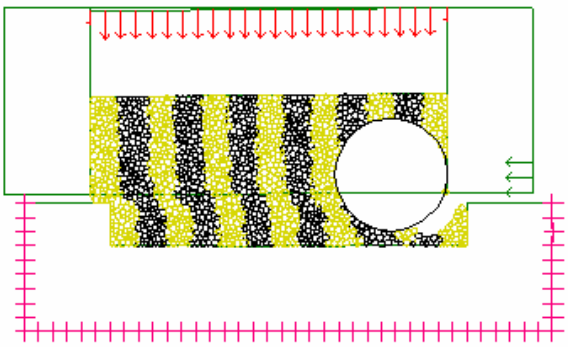

(d)

Figure 29: Numerical deformed samples with the applied normal stress of 68.2 kPa after 3.5 mm shear displacement: a) without the oversize cylinder, b) with the largest oversize cylinder placed on the left side of the box, c) with the largest oversize cylinder placed at the center of the box, and d) with the largest oversize cylinder placed on the right side of the box.

Note that in the situation without the oversize cylinder, all the deformed bands are approximately showing the same amount of shear distortion. On the other

hand, the shear distortion is not uniform along the shear band when the largest oversize particle is placed in the shear box. This is particularly true when the oversize cylinder is placed on the left side of the box. In fact, in this latter case, the third dark band from the left does not show any noticeable shear distortion. Therefore, the presence of oversize particle can prevent shearing distortion of the sample in some locations.

In Figures 30a to 30d, the displacement vectors of the cylinders for the situations in which there is no oversize cylinder and when the oversize cylinder was placed on the left side, at the center, and on the right side of the box are shown. Figure 30b shows a distinct deformation pattern compared to that in Figure 30a; in Figure 30b a few failure wedges are formed. In particular, the triangular wedge ABC in Figure 30b pushes the BCD region upward causing excessive tilting of the top plate in this case compared to the situation with no oversize cylinder or when the oversize cylinder is placed on the right side of the box. The failure mechanism in Figure 30b is different from that in a normal direct shear test and it needs more energy to develop. In fact, in the situation of Figure 30b, the sample along side AB is under a passive pressure while the top plate behaves as a retaining structure. This explains the greater observed shear strength (Figure 25) and friction angle in this situation (table 1).

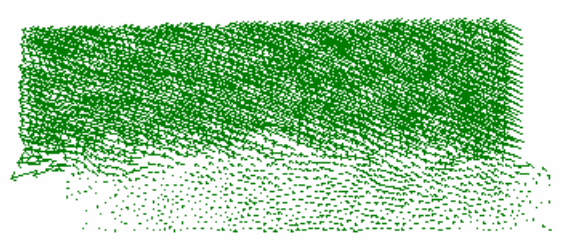

(a)

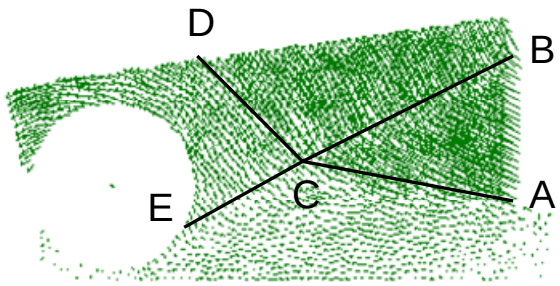

(b)

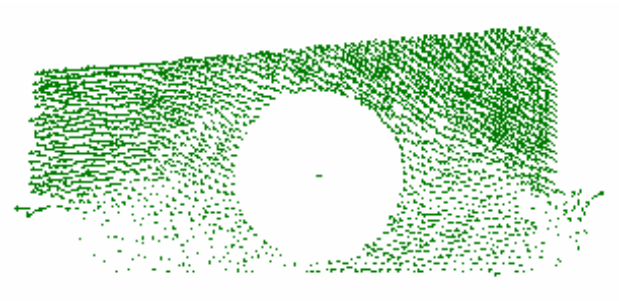

(c)

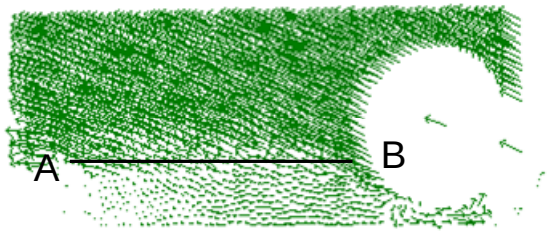

(d)

Figure 30: Numerical displacement field of the cylinders after 3.5 mm shear displacement under the normal stress of 68.2 kPa for the situation of a) no oversize cylinder and with the oversize cylinder placed b) on the left side of the box, c) at the center of the box, and d) on the right side of the box.

It is interesting to note that the direct shear test in Figure 30b can be approximately interpreted as a biaxial test if the peak applied pressure along side AB of the sample is considered as the axial stress (σ_1) and the pressure applied to the top plate is viewed as the confining stress (σ_3). Using the three pairs of σ_1 and σ_3 in the

three shear tests with the top plate pressures of (20.5, 42.3, and 68.2 kPa), and the Mohr-Coulomb failure criterion, i.e.

$$\sigma_1 = q_u + \sigma_3 \tan^2(\frac{\pi}{4} + \frac{\varphi}{2}) \tag{18}$$

a friction angle of φ = 41.0° and a cohesion of 5.8 kPa were obtained that are comparable to the friction angle of 41.2° and cohesion of 11.5 kPa from a shear test with no oversize cylinder. Note that q_u in equation 18 is the uniaxial compressive strength.

In Figures 31a and 31b, the friction angle and cohesion versus the normalized cylinder diameter are shown. Numerical results show an increase in friction angle and a decrease in cohesion (except when the largest cylinder is placed on the left side of the box) as the diameter of oversize particle increases. Note also that for the samples with the largest oversize cylinder, the resulted friction angles and cohesions show more variation as the location of the oversize cylinder is changed. In Figures 31a and 31b, the recommended limit of the maximum particle size to the box width of 0.1 by ASTM is shown as well.

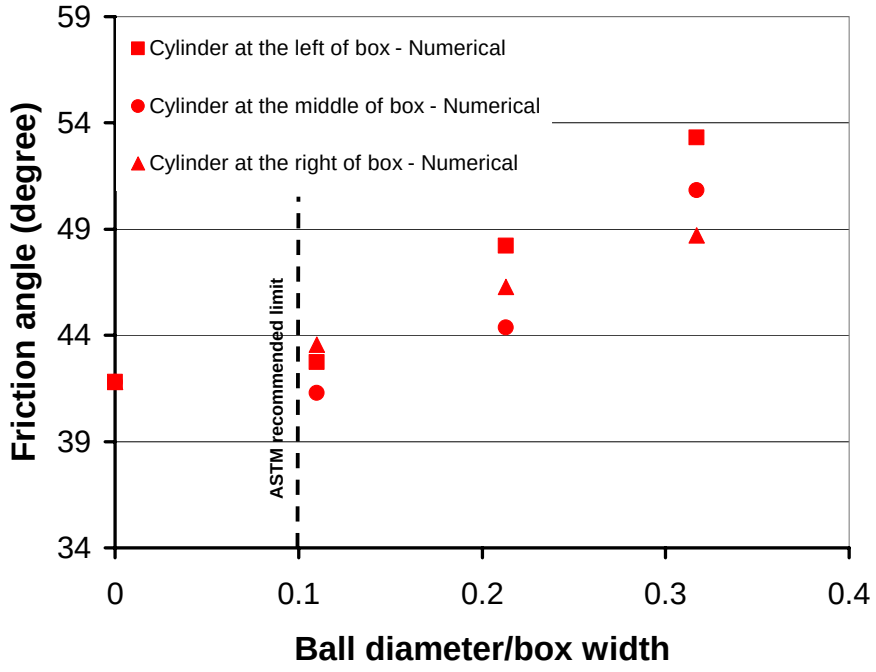

(a)

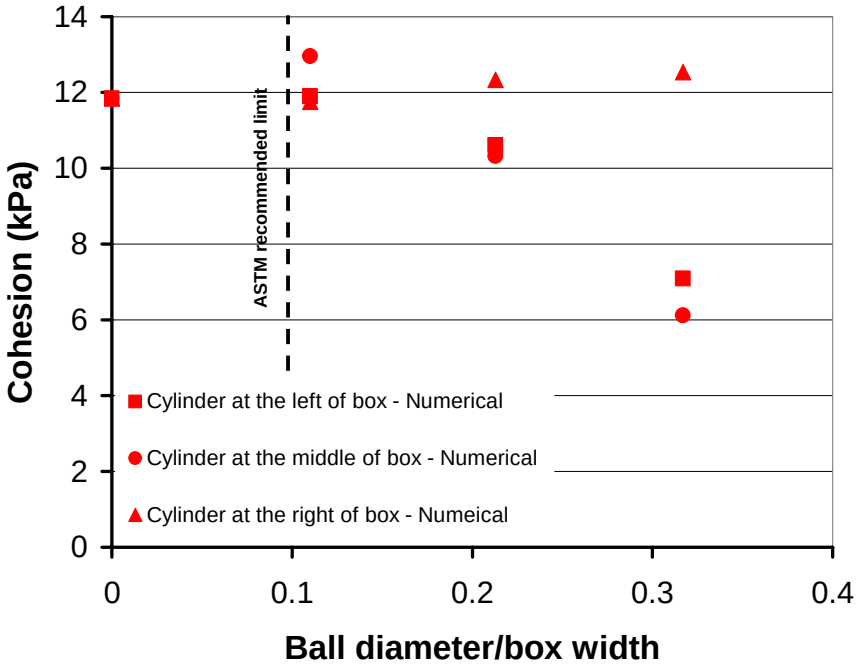

(b)

Figure 31: Friction angle (a) and cohesion (b) vs. the normalized oversize cylinder diameter.

6. Conclusion

The numerical results suggest that the internal failure mechanism of the material in a direct shear test can be affected if the oversize particle is too big (a ball of 1.90 cm in diameter in this study). The presence of oversize particle in general causes a non-uniform distribution of shear distortion within the sample, an increase in the measured friction angle and a decrease in the measured cohesion. Furthermore, it appears that a maximum particle size to box width of 0.2 can be used in direct shear testing without too much loss in accuracy of the measured friction angle and cohesion for the Questa rock pile material under the applied low normal stresses that were used in this study. The limit of 0.2 for the ratio of the largest particle size to the box width is greater than that of 0.1 recommended by ASTM standard D3080-98.

CHAPTER 4
Numerical Modeling of the *In-situ* Direct Shear Box

1. Introduction

In the previous chapters, both the laboratory direct shear tests on Questa rock pile material and the numerical simulations of the laboratory direct shear tests were reported. In this chapter, the numerical analysis of the *in-situ* shear box is studied. The *in-situ* shear box was 60 cm × 60 cm in size. During the *in-situ* direct shear tests, oversize rock fragments were observed in some of the rock pile blocks that can modify the measured shear strengths. This *in-situ* testing procedure is time-consuming and expensive if studied experimentally in the large scale. In the previous chapters, it was shown that the numerical model used is reliable as it produced results consistent with the laboratory findings. Therefore, the numerical technique should help predict the role of an oversize particle in the *in-situ* shear box tests.

The *in-situ* shear box used for the field tests is shown in Figure 32. The shear box is unlike to the conventional shear boxes, in that it is made only of a half box. The second half of the box is the semi-infinite soil domain underneath the box. The shear

box has dial gages for measuring shear and normal deformations and hydraulic jacks to apply the normal and shear forces. More detail about the *in-situ* shear box is in Fakhimi et al. (2008).

Figure 32: *In-situ* shear box set up in the field.

2. Numerical Modeling of the *In-situ* Direct Shear Box

The *in-situ* shear box model is made of four pieces that were modeled using finite elements; the vertical sides (AB and DC), the top plate (BC), and the region (ABCD) that connects the vertical sides AB and CD through the interfaces (see chapter 3 for more explanation). The top plate CB is in contact with the vertical side AB through an interface. No interface was defined between the top plate and vertical side CD to allow free rotation of the top plate. The interface between the top plate and the box side AB has no cohesion and friction to provide additional freedom to movement and rotation of the top plate, and to help to fully transfer the applied normal stress to the simulated soil sample. Internal surfaces of the box are defined as "walls" to allow interaction between the discrete elements and finite elements. Note that bottom edges of sides CD and BA of the box were defined as wall too.

In addition to the shear box, the surrounding far field material also was modeled. The domain HGFEDCBAJI was simulated by discrete elements while the domain encompassing this region was modeled as a continuum domain with an elastic behavior. The lengths in Figure 33 are: h_1 = 32 cm, h_2 = 120 cm, W_1 = 60 cm, W_2 = 240 cm and S = 14 cm. The three circles along the shear band in Figure 33 illustrate the different locations of the oversize particle considered in this study. The thickness of the vertical sides and top plate of the numerical shear box is 5 cm while the thickness of the *in-situ* shear box in reality is 0.5 cm. The thickness of the body of the numerical shear box was increased for two reasons. The increase in the thickness allowed us to have a better aspect ratio for the finite elements used to model the box. Furthermore, the greater thickness of the box helped to reduce the modulus of the box. Therefore, the difference between the elastic modulus of the shear box and the simulated rock pile material was reduced to induce faster convergence of the explicit numerical solution.

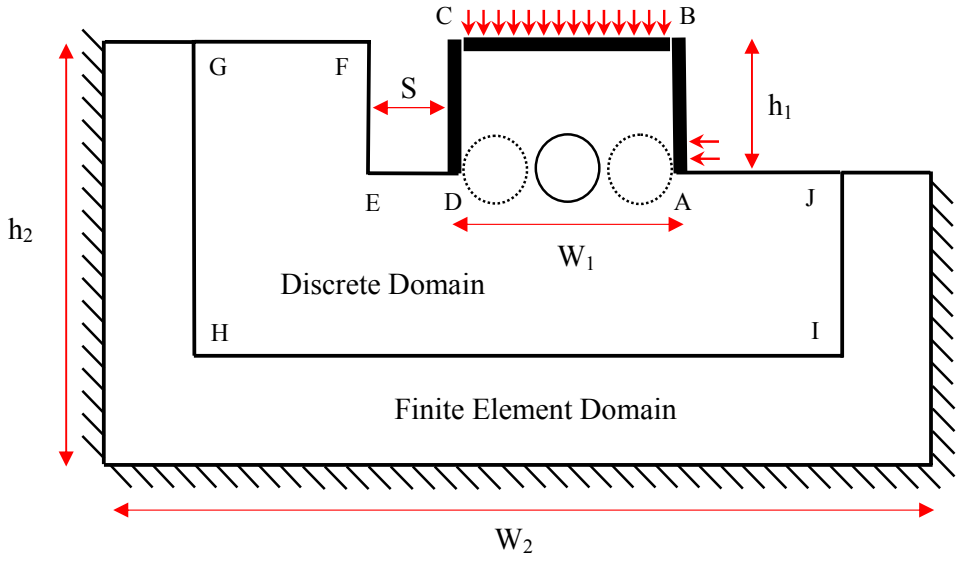

Figure 33: A sketch of *in-situ* direct shear box ABCD and far field material.

The logic and procedure for numerical modeling of the *in-situ* shear box is the same as those of laboratory scale shear box, which is presented in more detail in Chapter 3. Here, only issues that are specific to the *in-situ* shear box model are presented.

The micro-mechanical parameters for the *in-situ* shear test model were obtained using an elastic modulus of E = 16.8 MPa, a Poisson's ratio of $\nu = 0.2$, a friction angle of 41.2°, and a cohesion intercept of 11.5 kPa. Using the cylinders radii (R) of 4.7 to 9.5 mm, the calibration procedure resulted in the following micro-mechanical parameters:

k_n = 33.1 MPa, k_s = 7.6 MPa, n_b = 400 N/m, s_b = 400 N/m, $\mu = 1.0$, and σ_0/k_n=0.040-0.043.

These micro-properties together with cylinder-wall contact properties of k_n = 100.0 GPa, k_s = 100.0 GPa, $\mu = 0.5$, and $n_b = s_b = 0.0$ were used in the simulation of an *in-situ* direct shear test. The simulation confirmed that the selected micro-properties were in fact able to reproduce the correct macro-properties (E = 16.8 MPa, $\nu = 0.2$, $\varphi = 40.3°$, and c = 18.0 kPa) with an exception for the cohesion intercept that was 18.0 kPa compared to the target cohesion of 11.5 kPa. No attempts were made to adjust the micro-parameters to result in a better cohesion as the numerical simulations were time consuming. Besides, the cohesion of 18 kPa is within the range of cohesion values measured in the field.

Note the cylinders radii of 4.7 to 9.5 mm or cylinders diameters of 9.4 to 19.0 mm used for the numerical simulations are greater than the D_{50} = 0.9 mm of laboratory gradation curve and D_{50} = 4.8 mm of *in-situ* gradation curve of Spring Gulch material. The cylinders radii were chosen larger than the above D_{50}s to reduce the number of cylinders involved in the numerical simulations and to reduce the

computation time. The total number of discrete elements used for a numerical simulation without the oversize particle was 6070 cylinders.

The oversize cylinders 6.6 cm, 12.8 cm, and 19.0 cm in diameter were placed along the shear plane. To place the oversize particle in the shear box, the cylinders at the location of the oversize particle are excavated and then the oversize particle is generated. This approach helps to preserve the microscopic structure of the discrete system and should reduce the discrepancies in the results of numerical tests due to the fabric change (Koyama and Jing, 2007). Normal stresses of 20.5, 42.3, and 68.2 kPa (Similar to those for *in-situ* shear tests) were used for the numerical simulations. The normal stress on the shear plane is made of the effect of weight of the simulated soil block and the applied normal stress to the top plate. The density of discrete cylinders was assumed as 1900 Kg/m^3. After sample preparation that follows similar procedure as described in the previous chapter, the problem is solved for gravitational effects. Additional normal forces to the top plate of the shear box (Figure 33) is applied such that the total normal stress at the shear plane (made of the block weight and the applied normal stress to top plate) to be equal to the desired normal stress. The shear force was induced in the system by applying a constant velocity of 4.5×10^{-9} m/numerical cycle to the bottom part of wall AB that is shown with arrows in Figure 33. The applied velocity was small enough to result in a quasi-static solution of the problem.

3. Numerical Test Results

The shear stress versus shear displacement from the numerical shear tests for the situations that the oversize cylinder is placed on the left side, at the center, and on the right side of the box with the normal stress of 68.2 kPa are shown in Figures 34a,

34b, and 34c, respectively. These Figures illustrate that the presence of oversize particle in the *in-situ* box model does not change the shear strength significantly. In addition, the location of the oversize particle does not significantly affect the shear strength of the material. However, it is interesting to note that the effect of oversize particle's location is more pronounced during the initial deformation of the material. Specifically, it is clear that the effect of presence of oversize particle during the shear testing appears earlier when it is located on the right side of the box compared to the case that oversize particle is placed on the left side of the box. Nevertheless, the final peak shear strength is not much affected by the location of oversize particle. Generally, a little higher shear strength is observed when the oversize particle is placed at both sides of the box (left and right). In fact, shear strength is increased by 6.7% to 13.2% (from 80.9 kPa to 85.8 kPa), 1.3% to 7.8% (from 76.8 kPa to 81.7 kPa), and 5.7% to 16.0% (from 80.1 kPa to 87.9 kPa) compared to that with no oversize particle (75.8 kPa), when the oversize particles are placed on the left, at the center, and on the right side of the box, respectively. It is also interesting to note that the maximum increase in the shear strength is not greater than 16%.

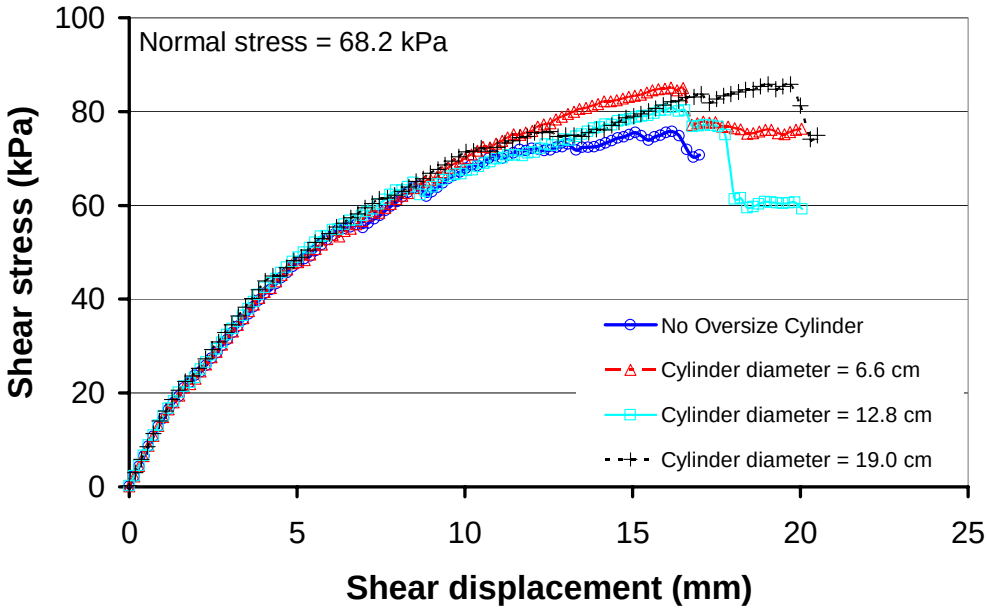
Normal stress = 68.2 kPa
Shear stress (kPa)
Shear displacement (mm)
0
20
40
60
80
100
0
5
10
15
20
25
No Oversize Cylinder
Cylinder diameter = 6.6 cm
Cylinder diameter = 12.8 cm
Cylinder diameter = 19.0 cm

(a)

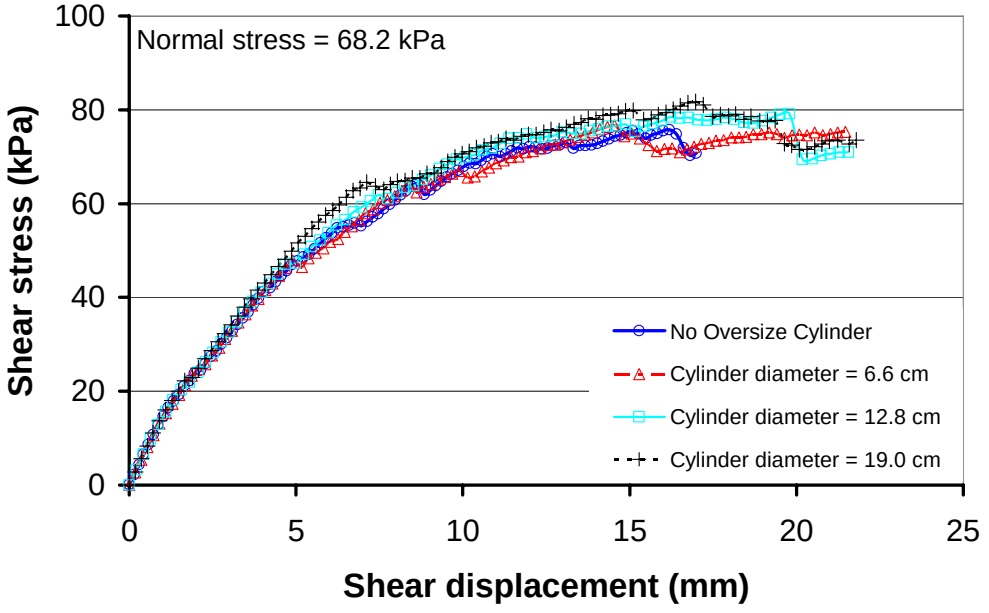
Normal stress = 68.2 kPa
Shear stress (kPa)
Shear displacement (mm)
0
20
40
60
80
100
0
5
10
15
20
25
No Oversize Cylinder
Cylinder diameter = 6.6 cm
Cylinder diameter = 12.8 cm
Cylinder diameter = 19.0 cm

(b)

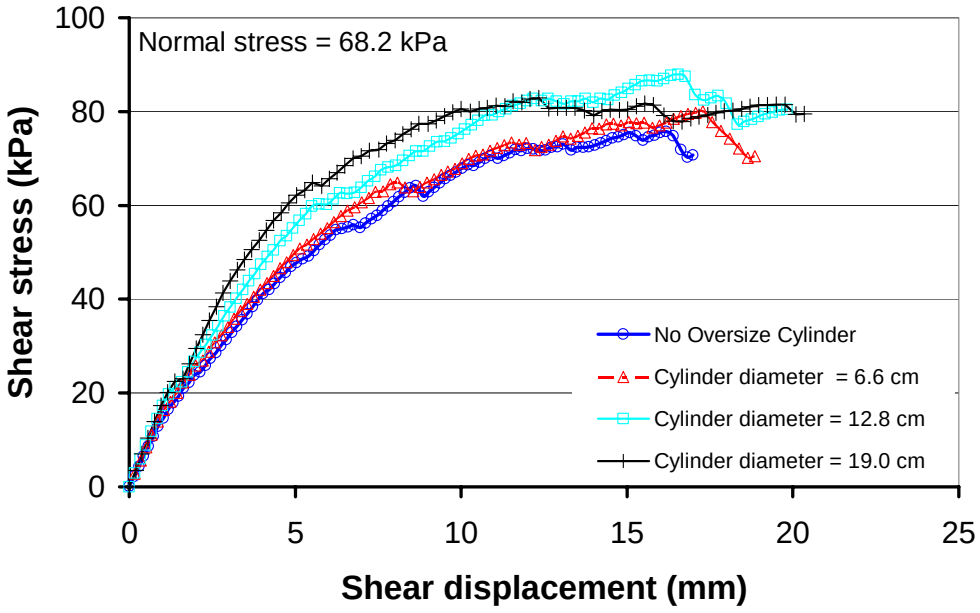

(c)

Figure 34: Shear stress vs. shear displacement of the numerical shear tests with the applied normal stress of 68.2 kPa for the oversize cylinder placed a) on the left side, b) in the middle, and c) on the right side of the box.

Micro-cracks in the numerical simulations, with the normal stress of 68.2 kPa after about 20 mm shear displacement for the shear tests without the oversize cylinder and with the largest cylinder (19.0 cm in diameter) placed on the left side, at the center, and on the right side of the box, are shown in Figures 35a, 35b, 35c, and 35d, respectively. It is observed that damaged region around the shear band and the crack patterns are generally the same and do not show significant differences. The exception is for the case that the oversize particle is located on the left side of the box (Figure 35b) in which the micro-cracks appear to be more extensive.

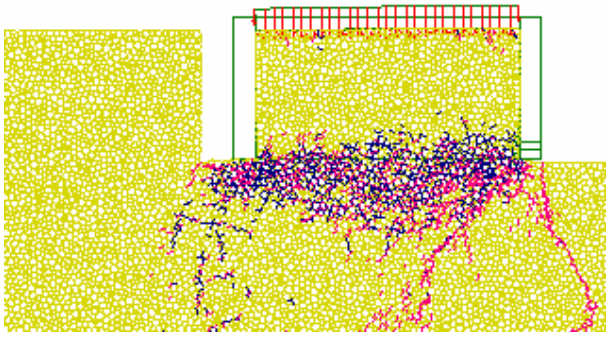

(a)

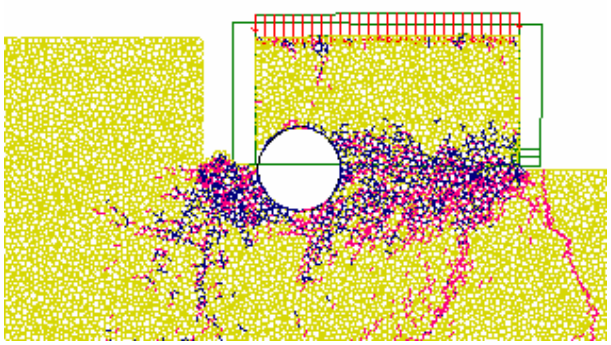

(b)

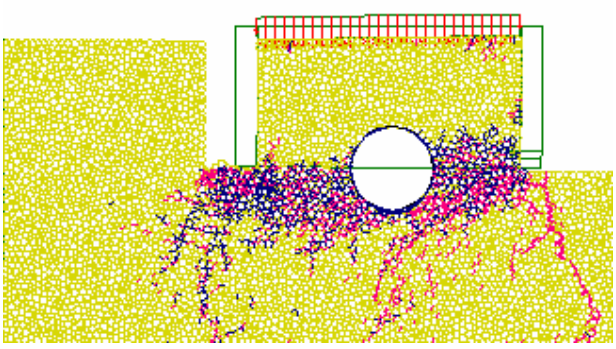

(c)

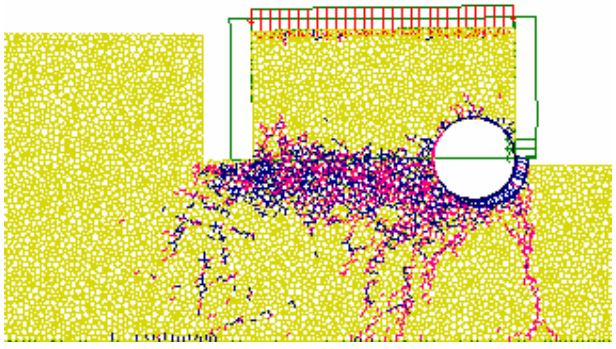

(d)

Figure 35: Micro-cracks in the numerical samples with the applied normal stress of 68.2 KPa after 20 mm shear displacement for the sample a) without the oversize cylinder, b) with the largest oversize cylinder on the left side of the box, c) with the largest oversize cylinder placed at the center of the box, and d) with the largest oversize cylinder placed on the right side of the box. Tensile and shear cracks are in red and blue, respectively.

In Figures 36a to 36d, the displacement vectors of the cylinders for the situations that no oversize particle is in the box and the oversize cylinder is placed on the left side, at the center, and on the right side of the box are shown. The figures suggest no significant difference in the deformational patterns for these four situations.

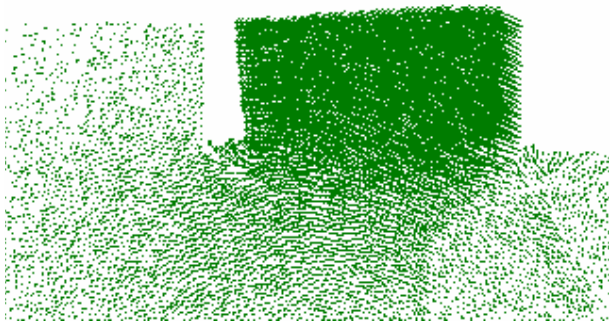

(a)

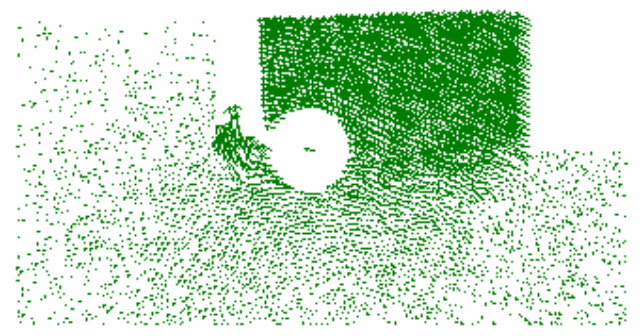

(b)

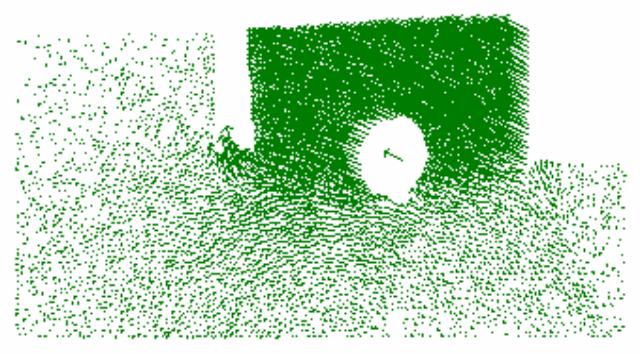

(c)

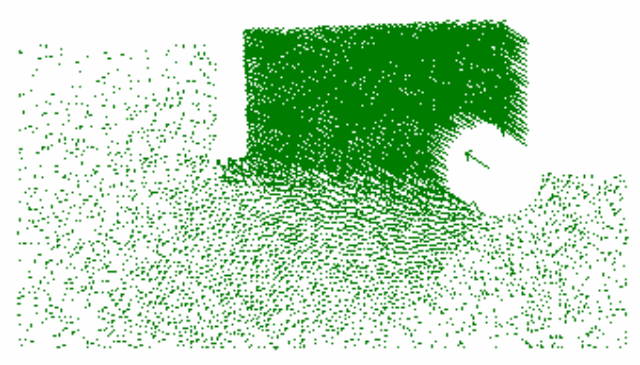

(d)

Figure 36: Numerical displacement field of the cylinders after 20 mm shear displacement under the normal stress of 68.2 kPa a) without the oversize particle, and with the oversize particle placed b) on the left side, c) on the right side, and d) at the center of the box.

In Figures 37a and 37b, the friction angle and cohesion versus the normalized cylinder diameter (ratio of cylinder's diameter to W_1 in Figure 33) are shown. From these graphs, it is observed that the average friction angle does not show a significant change due to the presence of oversize particle. The effect of oversize particle on the average cohesion is small as well. Overall, some variations in the simulated friction angle and cohesion values by changing the size and location of oversize particle are observed, but they are most likely due to the natural variations in a chaotic system such as the discrete element model used for this problem.

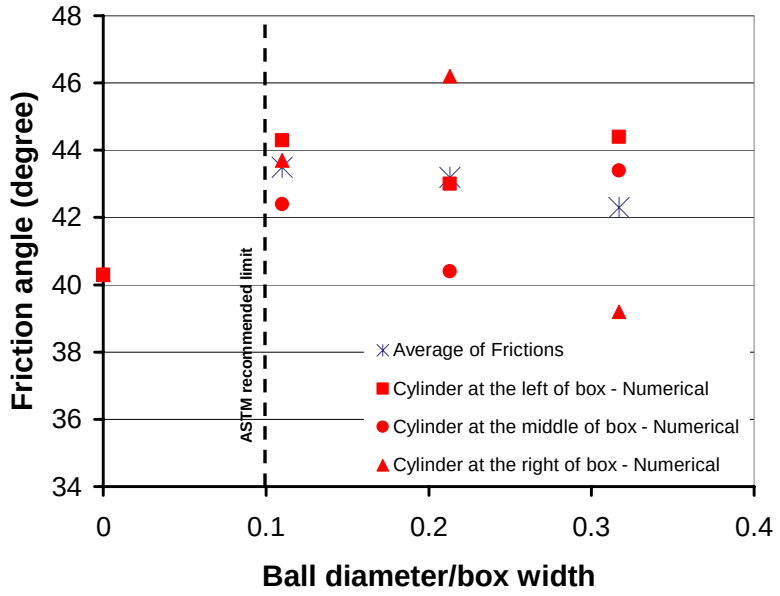

(a)

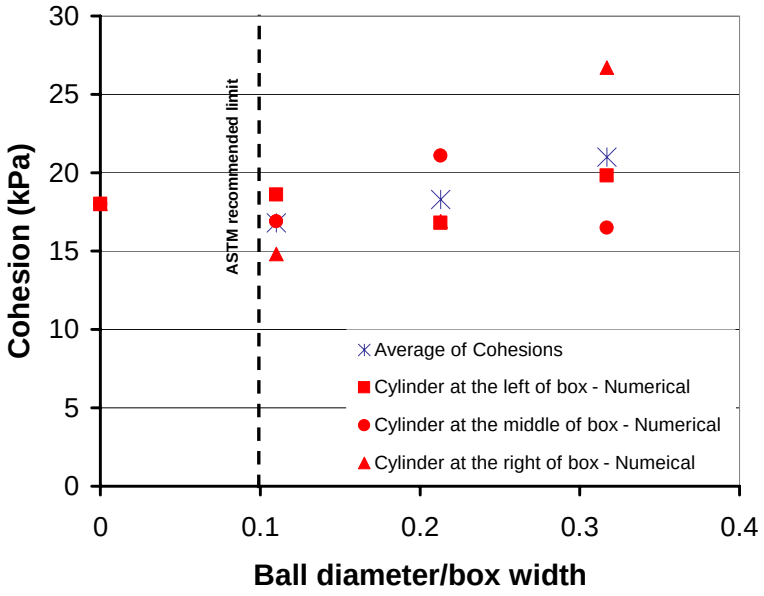

(b)

Figure 37: Cohesion (a) and friction angle (b) vs. the normalized oversize cylinder diameter.

4. Conclusion

Numerical modeling of the *in-situ* shear test was performed to investigate the effect of an oversize particle on the shear strength of material. The results suggest that the presence of an oversize cylinder in the shear box has small effect on the simulated friction angle and cohesion values. The reasons that the oversize particle in this model has less significant effect on the measured shear strength compared to that of laboratory box simulation are:

a) The width of the box was defined as W_1 in Figure 33. In reality, the second half of the shear box has a width of W_2 that is practically of infinite size. Therefore, the oversize cylinders used in our analysis of the *in-situ* shear tests are comparatively smaller than that in the situation of the laboratory test simulations.

b) The height of the *in-situ* shear box (h_1 or h_2) relative to the oversize cylinder diameter is comparatively greater than that of the laboratory box.

For the above reasons, the presence of an oversize particle seems to be mostly restricted to the small changes it makes to the micro-crack pattern. The change in the crack pattern could result in either a weaker or a stronger shear band pattern in the chaotic system such as the discrete element model used in our analysis. Previous studies have shown that changing the random particle distributions slightly with the same micromechanical parameters can result in some changes in the simulated friction angle (Koyama and Jing, 2007). Therefore, the changes in friction angles and cohesions reported in Figure 37 are mostly due to the chaotic effects. In the laboratory shear box simulations, the size of the oversize particle was big enough compare to the size of the box to dominate the shear behavior of the material and mask the chaotic effects. From practical point of view, it is important to notice that a normalized

oversize particle width of 0.2 does not affect the measured cohesion significantly. This is consistent with the conclusions made for the laboratory studies.

CHAPTER 5
CONCLUSION

1. Conclusion

Laboratory and numerical tests were performed to investigate the role of oversize particles on the shear strength of granular material. In particular, it was important to know how the large rock fragments observed in the *in-situ* shear test blocks of rock pile material change the measured friction angle and cohesion values.

In the laboratory testing, a shear box 6 cm × 6 cm in size was used. The material from Spring Gulch rock pile passed through #6 sieve was compacted with a moisture content of 6%. Normal stresses of 20.5, 42.3, and 68.2 kPa were used for the laboratory tests.

In the numerical simulations, the CA2 (Fakhimi, 1998) computer program was used. The rock pile material was simulated with discrete elements while the shear box was modeled with finite elements. For both the experimental and numerical tests, Mohr-Coulomb failure criterion was used to interpret the results.

In Figures 38a and 38b, the cohesion and friction angle values for both the laboratory and numerical tests are illustrated. It is clear that the numerical model results are consistent with those of laboratory tests. The only difference is that the

friction angles from the numerical model show more sensitivity to the presence of oversize particle.

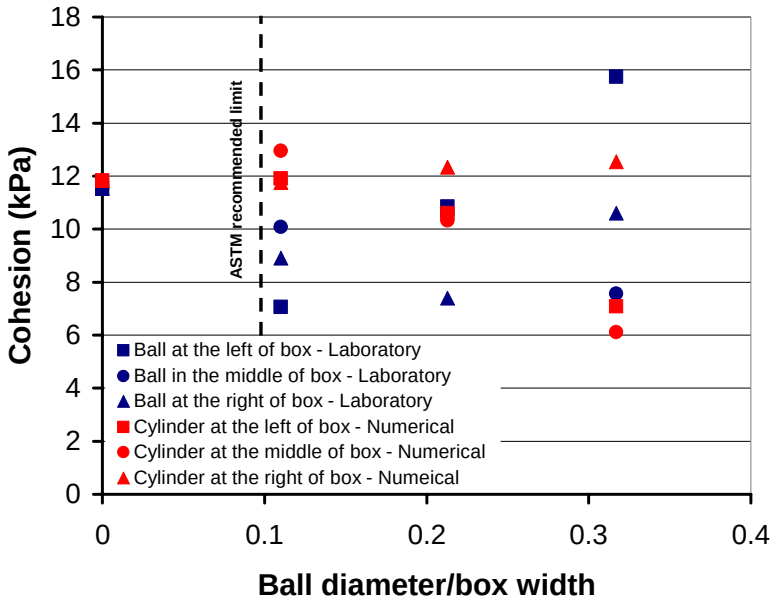

(a)

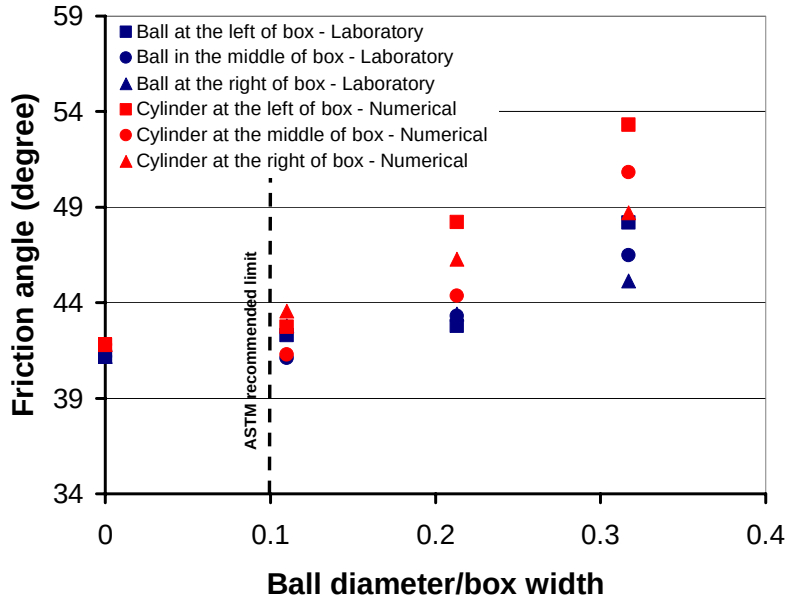

(b)

Figure 38: Cohesion (a) and friction angle (b) vs. the normalized oversize ball diameter obtained from laboratory and numerical direct shear test.

Table 3: The friction angles and cohesions from the physical and numerical tests. (D is the oversize particle diameter and W is the box width)

Diameter of oversize particle/ box width (cm)	*Location of the ball*	*Laboratory friction angle (Degree)*	*Numerical friction angle (Degree)*	*In-situ Numerical friction angle (Degree)*	*Laboratory cohesion (kPa)*	*Numerical cohesion (kPa)*	*In-situ Numerical cohesion (kPa)*
D/W = 0.3	Left	48.2	53.3	44.4	15.8	7.1	19.8
	Middle	46.5	50.8	43.4	7.6	6.1	16.5
	Right	45.1	48.7	39.2	10.6	12.5	26.7
D/W = 0.2	Left	42.8	48.2	43.0	10.8	10.6	16.8
	Middle	43.3	44.4	40.4	10.5	10.3	21.1
	Right	43.4	46.3	46.2	7.4	12.3	16.9
D/W = 0.1	Left	42.3	42.8	44.3	7.1	11.9	18.6
	Middle	41.1	41.3	42.4	10.1	13.0	16.9
	Right	42.8	43.6	43.7	8.9	11.8	14.8
No ball	N/A	41.2	41.8	40.3	11.5	11.8	18.0

Table 3 reports the friction angles and cohesions from the physical and numerical tests. The physical and numerical laboratory results suggest that both friction angle and cohesion are affected by the presence of oversize particles and their locations. Note also that the average friction angle and cohesion are not changed significantly in the numerical simulation of the *in-situ* shear box due to the presence of an oversized cylinder.

The results from the physical and numerical laboratory tests in Figures 38a and 38b, and Table 3 suggest that the average error in friction angle and cohesion measurement for a maximum particle size to box width of 0.2 are approximately 2 to 3 degrees and 10% to 15%, respectively. Therefore, it appears that the ASTM requirement is conservative for the Questa rock pile material, and a limit of 0.2 of the

ratio of maximum particle size to box width for the Questa rock pile material could be used in measuring the cohesion and friction angle without too much loss of accuracy.

As a result of this study, the normalized maximum allowable rock fragment size in the *in-situ* shear box was increased from 1/7 to 1/5. This allowed more *in-situ* direct shear tests to be considered as valid tests.

2. Proposed Future Work

The following research studies are proposed in continuation of this work:

1. Although the two dimensional numerical model used in this study could approximately mimic the behavior of Questa rock pile material, more accurate results could be obtained if a three dimensional simulation of the shear box is conduced.

2. In the numerical study, a brittle contact bond model was used. A softening micro-mechanical model should simulate the Questa rock pile material more accurately.

3. Laboratory tests with the *in-situ* shear box should help to more accurately verify the numerical findings in this thesis.

4. A discrete element simulation with angular particles (instead of circular particles) is recommended. Angular particles should simulate Questa rock pile material more realistically.

References

ASTM standard D3080-98 (2003). "Annual book of ASTM standards." Section four, Construction, Volume 04.08.

Becker, E., Chan, C. K., and Seed, H. B. (1972). "Strength and deformation characteristics of rockfill materials in plane strain and triaxial compression tests." Report No. TE 72-3 to State of California Department of Water Resources, Department of Civil Engineering, University of California Berkeley, California, USA.

Boakye, K., 2008, "Large in situ direct shear tests on rock piles at the Questa Mine, Taos County, New Mexico": M.S. thesis, New Mexico Institute of Mining and Technology, Socorro, 156 p.

Cerato, A. B. and Lutenegger, A. J. (2006). "Specimen size and scale effects of direct shear box tests of sands." Geotechnical Testing Journal, Vol. 29, No. 6, pp. 507-516.

Cundall, P. A., "A computer model for simulating progressive, large scale movements in blocky rock system." Proceedings of the International Symposium Rock Fracture, ISRM, Nancy, Paper No. II-8, vol. 1, 1971.

Cundall, P. A. and Strack O. D. L., "A discrete numerical model for granular assemblies." Geotechnique 29(1): 47-65, 1979.

Das, Braja M. (1985). "Principles of geotechnical engineering", PWS Engineering.

Fakhimi, A. (1998). "Theory and user manual of CA2 computer program." (in Farsi), Report No. 262, Building and Housing Research Center, Tehran, Iran.

Fakhimi, A. (2004). "Application of slightly overlapped circular particles assembly in numerical simulation of rocks with high friction angles." Engineering Geology, Vol. 74, pp. 129-138.

Fakhimi, A., Lin, Q., Haggerty, M., and Labuz, J.F. (2005). "Development of fracture in bending experiments." ARMA/USRMS 05-844, The 40th US Rock Mechanics Symposium, Anchorage, Alaska.

Fakhimi, A. and Villegas, T. (2007). "Application of dimensional analysis in calibration of a discrete element model for rock deformation and fracture." Rock Mech. Rock Engng., Vol. 40, no. 2, pp. 193-211.

Fakhimi, A., Boakye K., Sperling D., and McLemore V. (2008), "Development of a modified *in-situ* direct shear test technique to determine shear strength of mine rock piles", Geotechnical Testing Journal, Vol. 31, No. 3, pp. 1-5.

Gutierrez, L.A.F., 2006, "The influence of mineralogy, chemistry and physical engineering properties on shear strength parameters of the Goathill North rock pile material, Questa Molybdenum mine, New Mexico": M. S. thesis, New Mexico Institute of Mining and Technology, Socorro, 201 p., http://geoinfo.nmt.edu/staff/mclemore/Molycorppapers.htm, accessed December 06, 2007.

Hennes, R. G. (1952) "The strength of gravel in direct shear." ASTM special technical publication, Vol. STP 131, pp. 51-62.

Holtz, W. G. and Gibbs H. J. (1956). "Triaxial shear tests on pervious gravelly soils." Journal of the Soil Mechanics and Foundation Division; Proceedings of the American Society of Civil Engineers, Vol. 82, pp. 1-22.

Itasca Consulting Group, Inc. (1999). "PFC2D, particle flow code in 2 dimensions." Minneapolis, MN, USA.

Kirkpatrick, W.M., (1965). "Effect of grain size and grading on the shearing behavior of granular materials.", Proceedings of the sixth International Conference on Soil Mechanics and Foundation Engineering, Montreal, Canada.

Koyama, T. and Jing, L. (2006). "Effect of model scale and particle size on micro-mechanical properties and failure processes of rocks – A particle mechanics approach." Journal of Engineering Analysis with Boundary Elements 31, pp. 458-472.

Leslie, D. D. (1963). "Large-scale triaxial tests on gravelly soils." Pan-American Conference on Soil Mechanics and Foundation Engineering, Vol. 1, pp. 181-202.

Nieble, C. M., Silveira, J.F., and Midea, N. F. (1974). "Some experiences on the determination of the shear strength of rock fill materials." Proceedings of the Second International Congress of the International Association of Engineering Geology, Sao Paulo, Brazil, pp. IV-34.1-12.

Rathee, R. K. (1981). "Shear strength of granular soils and its prediction by modeling techniques." Journal of the Institution of Engineers (India), Part C1, Civil Engineering Division, Vol. 62, Special Issue on Hydrology and Hydraulic Engineering, pp. 64-70.

Simoni, A. and Houlsby, G. T. (2006). "The direct shear strength and dilatancy of sand-gravel mixtures." Geotechnical and Geological Engineering, 24, pp. 523-549.

Su, W. (1989). "Static strength evaluation of cohesionless soils with oversize particles." PhD dissertation, Washington State University, Pullman, WA.

APPENDIX A

Laboratory Shear Test Results

Complementary Experimental results for normal load of 20.5 kPa and 42.3 kPa.

Shear stress vs. shear displacement for normal load 20.5 kPa:

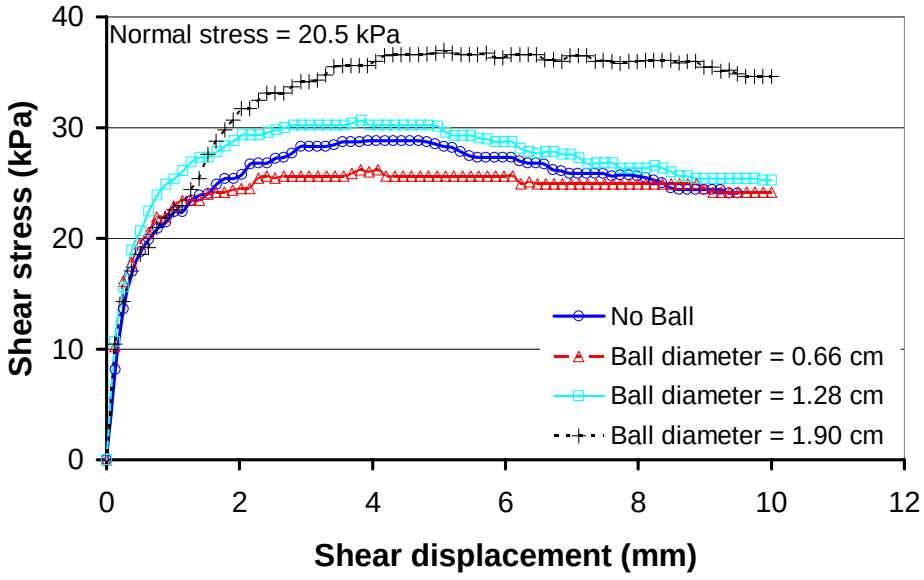

Figure A - 1: Shear stress vs. shear displacement for the steel ball placed on the left side of the box.

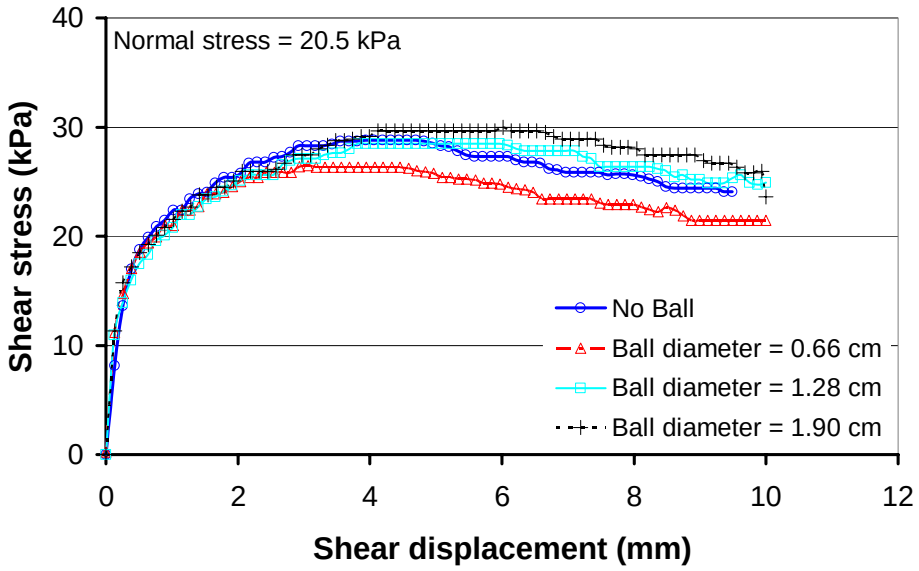

Figure A - 2: Shear stress vs. shear displacement for the steel ball placed in the middle of the box.

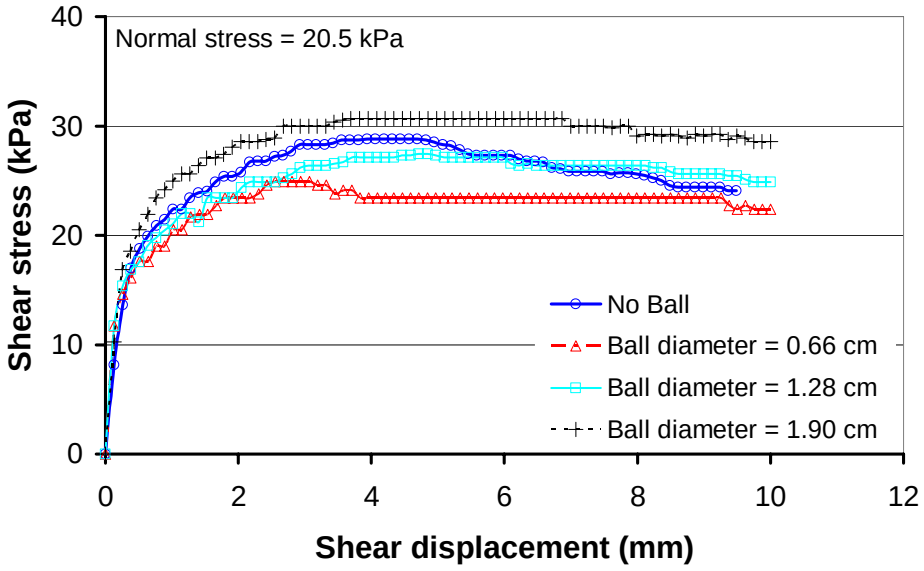

Figure A - 3: Stress vs. shear displacement for the steel ball placed on the right side of the box.

Dilation (Vertical displacement vs. shear displacement) for normal load of 20.5 kPa:

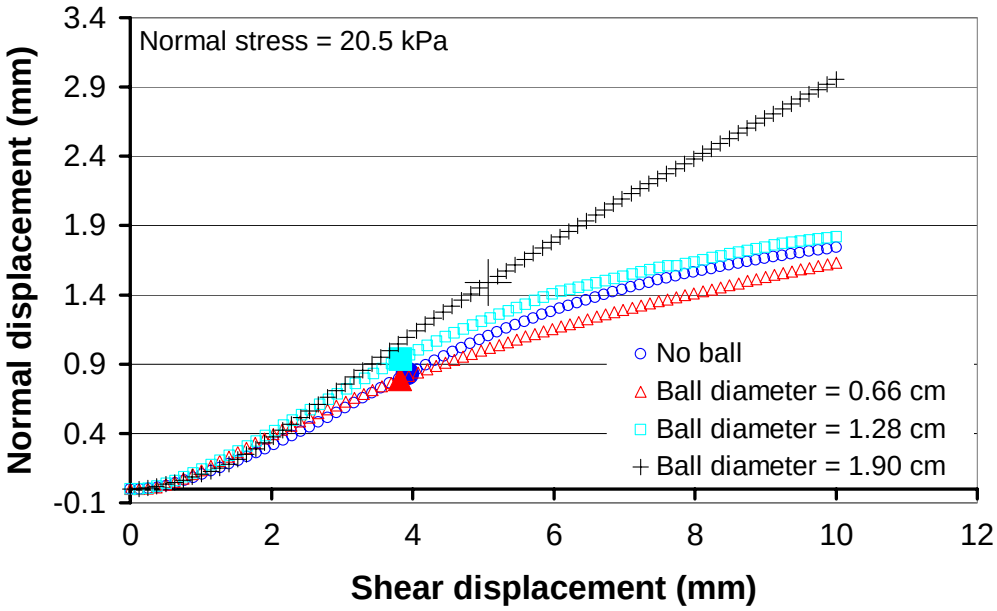

Figure A - 4: Normal displacement vs. shear displacement for the samples with the steel ball located on the left side of the box.

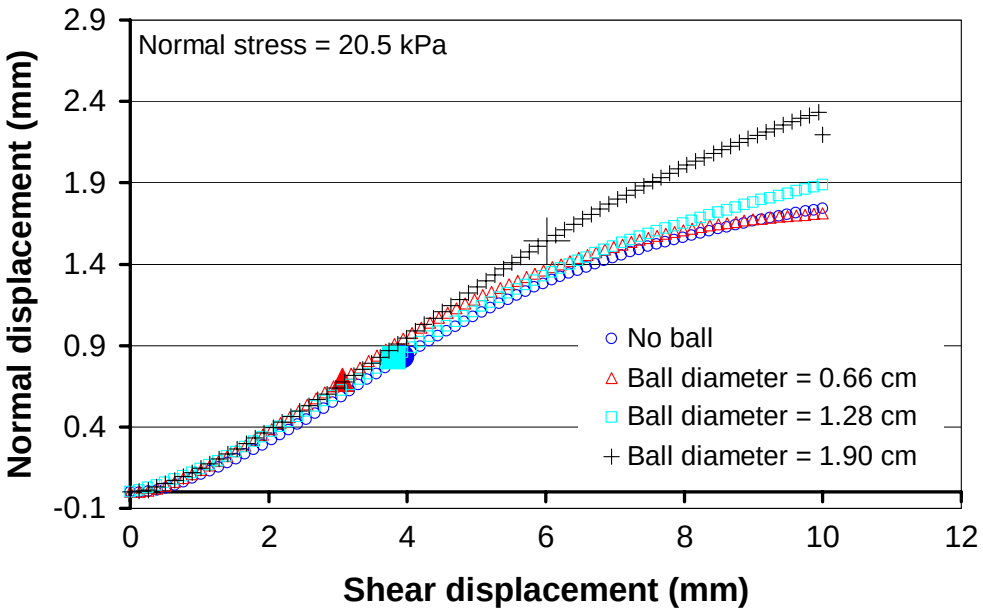

Figure A - 5: Normal displacement vs. shear displacement for the samples with the steel ball located in the middle of the box.

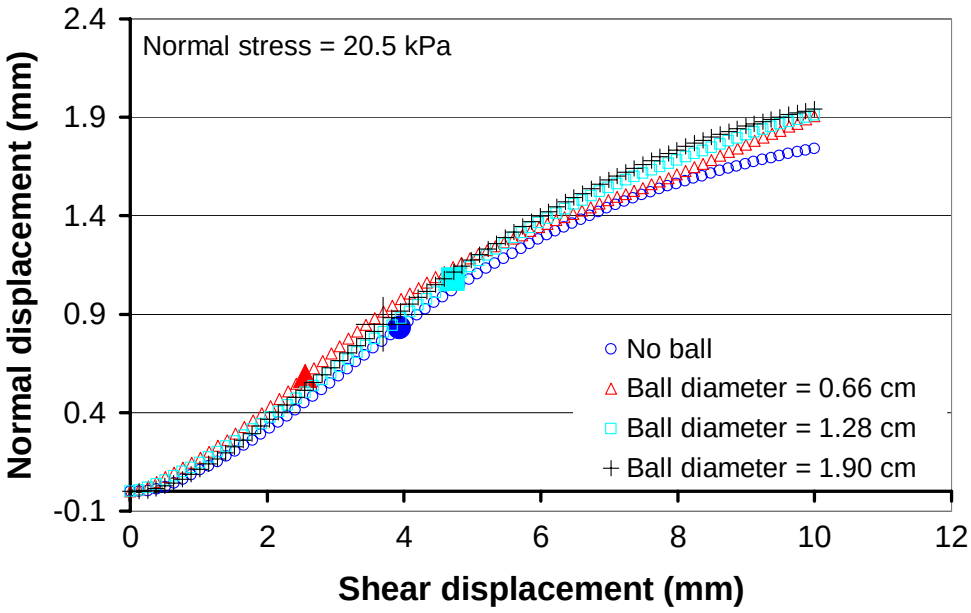

Figure A - 6: Normal displacement vs. shear displacement for the samples with the steel ball located on the right side of the box.

Shear stress vs. shear displacement for normal load 42.3 kPa:

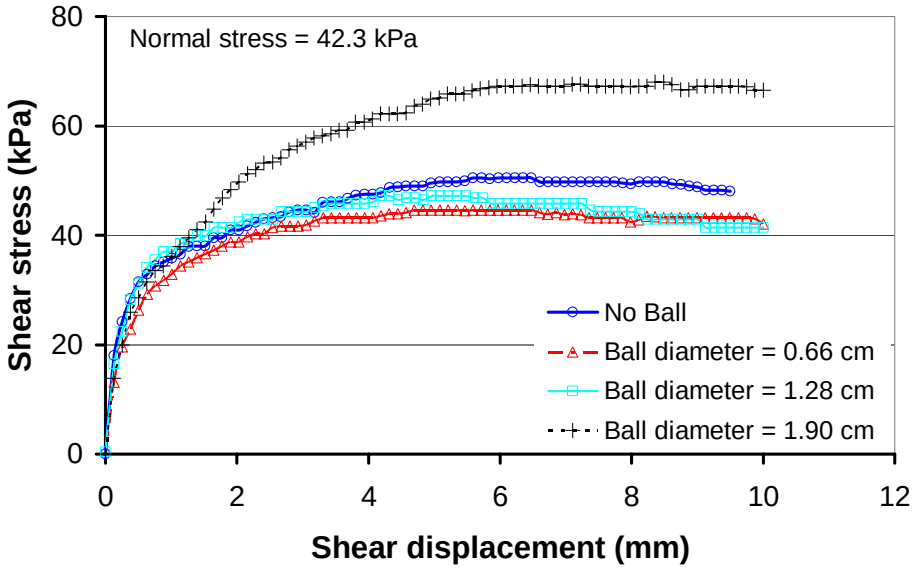

Figure A - 7: Stress vs. shear displacement for the steel ball placed on the left side of the box.

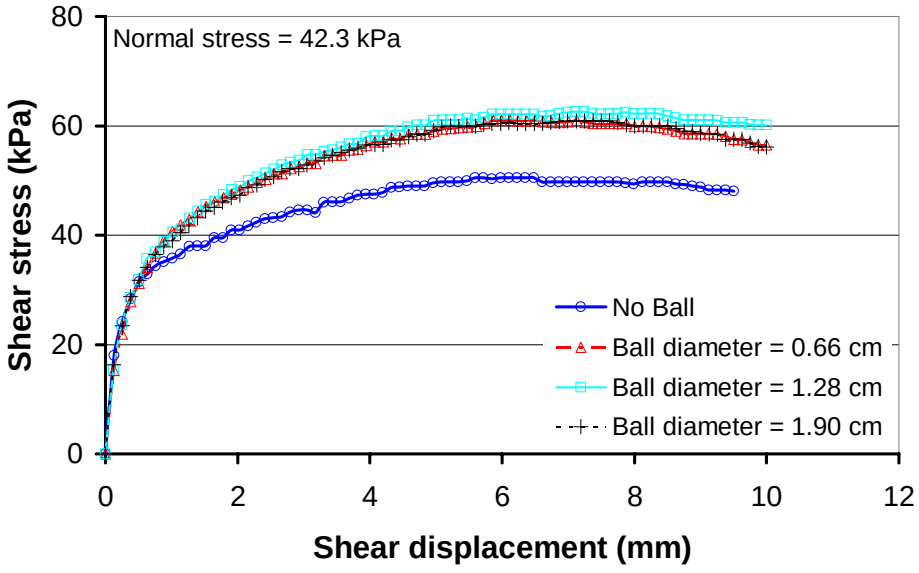

Figure A - 8: Stress vs. shear displacement for the steel ball placed in the middle of the box.

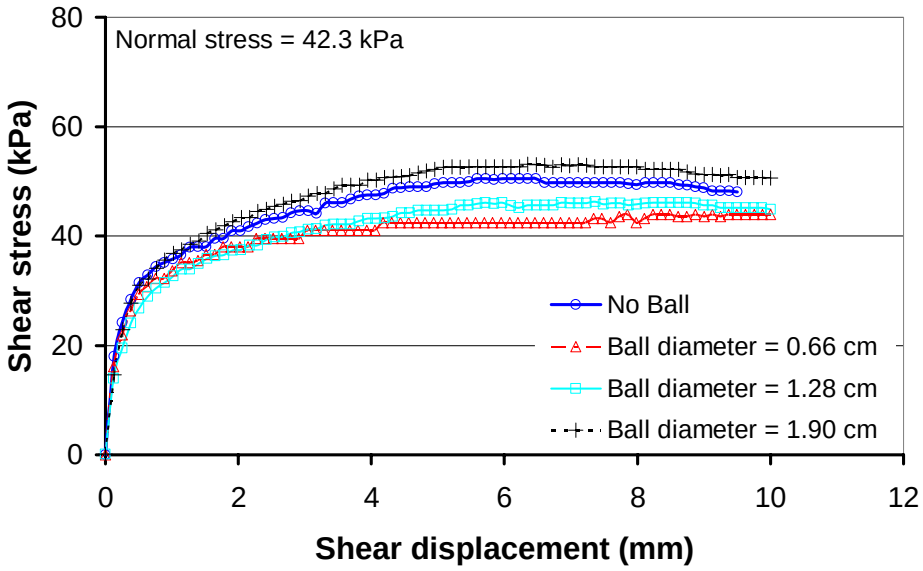

Figure A - 9: Shear stress vs. shear displacement for the steel ball placed on the right side of the box.

Dilation (Vertical displacement vs. shear displacement for normal load of 42.33)

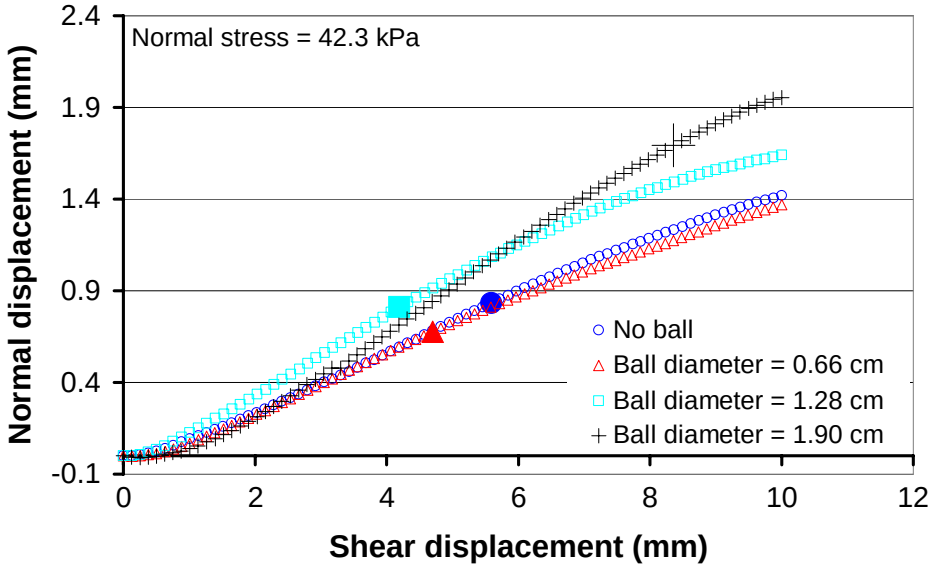

Figure A - 10: Normal displacement vs. shear displacement for the samples with the steel ball located on the left side of the box.

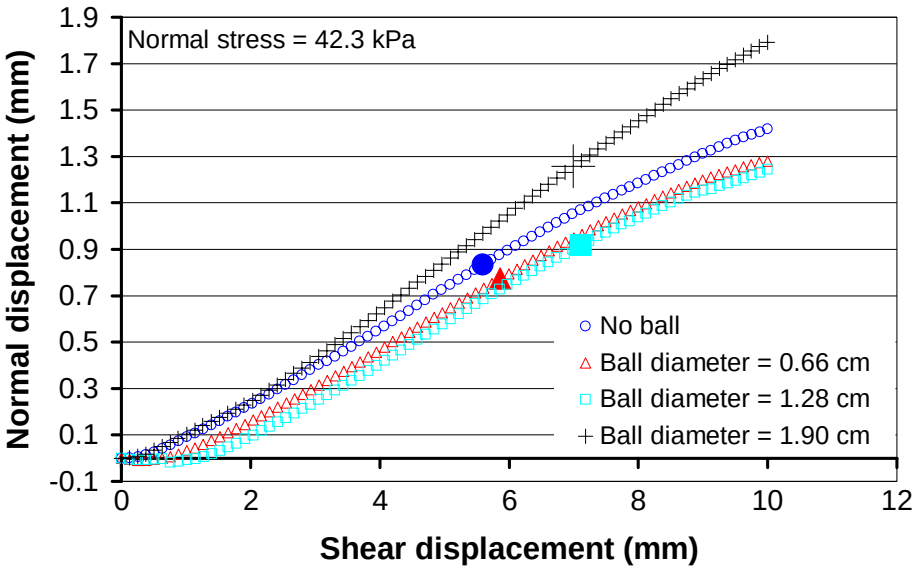

Figure A - 11: Normal displacement vs. shear displacement for the samples with the steel ball located in the middle of the box.

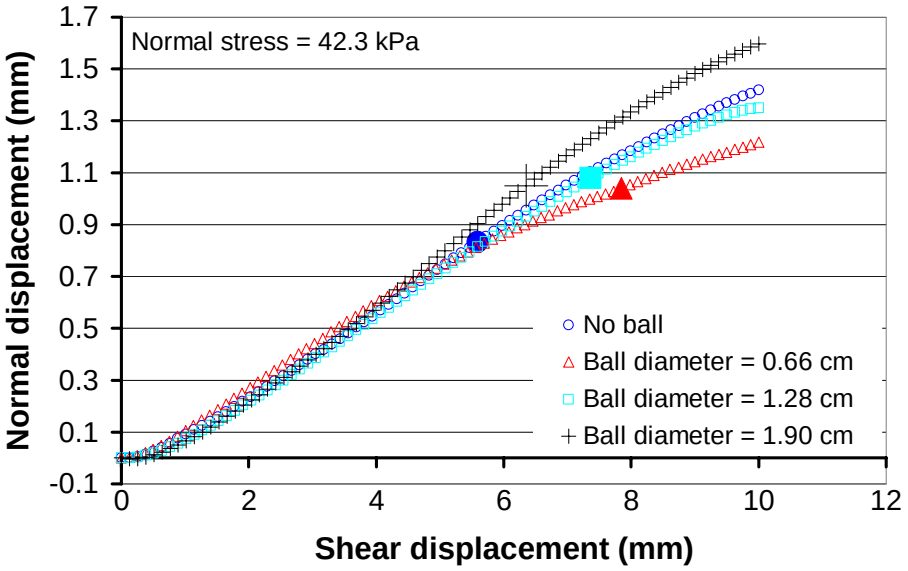

Figure A - 12: Normal displacement vs. shear displacement for the samples with the steel ball located on the right side of the box.

APPENDIX B

Results of Numerical Simulation of Laboratory Shear Box

Complementary numerical results for normal load of 20.5 and 42.3 kPa.

Shear stress vs. shear displacement for normal load of 20.5 kPa:

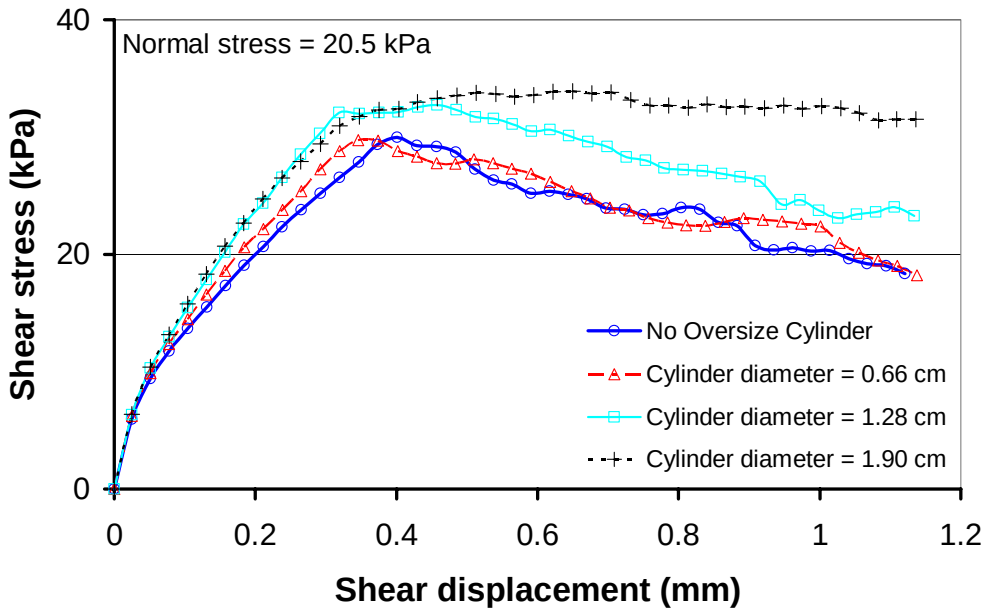

Figure B - 1: Shear stress vs. shear displacement of the numerical shear tests with the applied normal stress of 20.5 kPa for the oversize cylinder placed on the left side of the box.

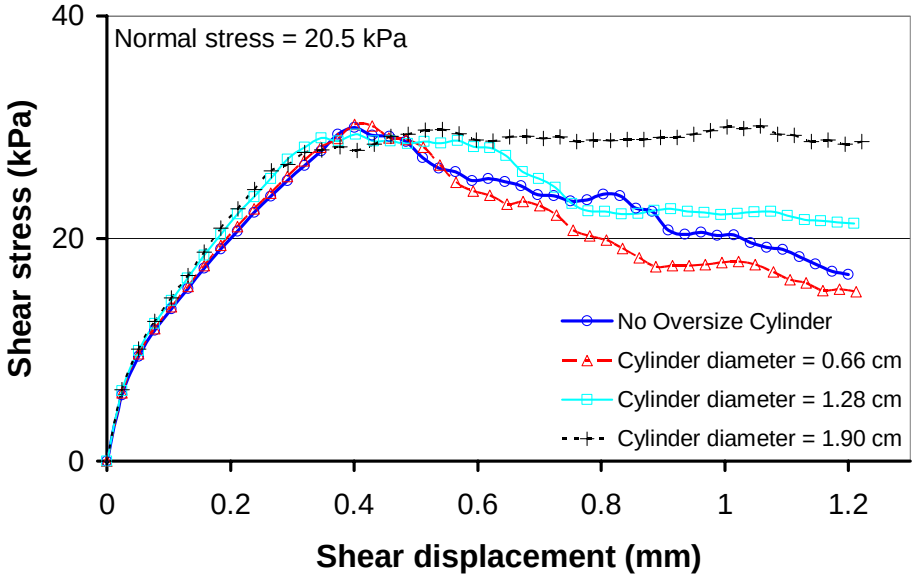

Figure B - 2: Shear stress vs. shear displacement of the numerical shear tests with the applied normal stress of 20.5 kPa for the oversize cylinder placed in the middle of the box.

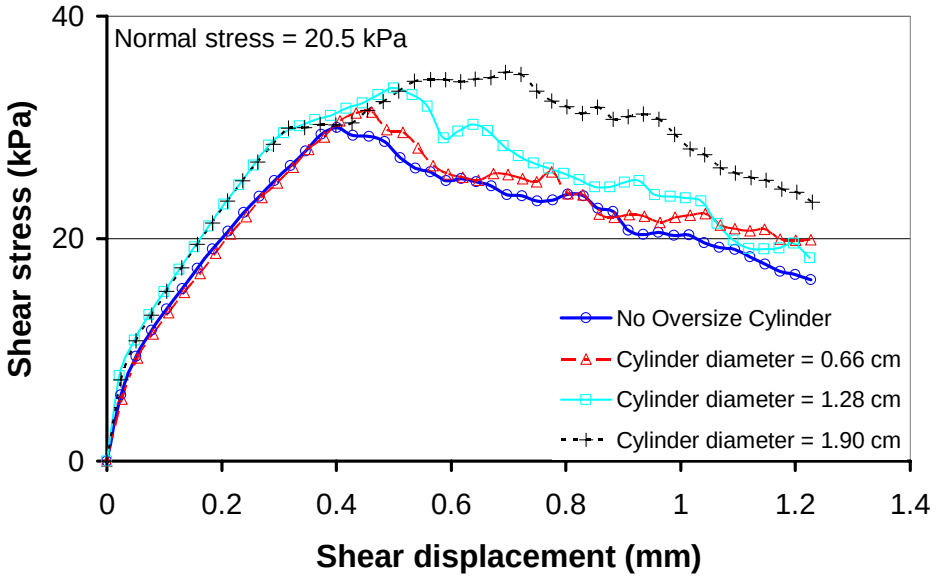

Figure B - 3: Shear stress vs. shear displacement of the numerical shear tests with the applied normal stress of 20.5 kPa for the oversize cylinder placed on the right side of the box.

Shear stress vs. shear displacement for normal load of 42.3 kPa:

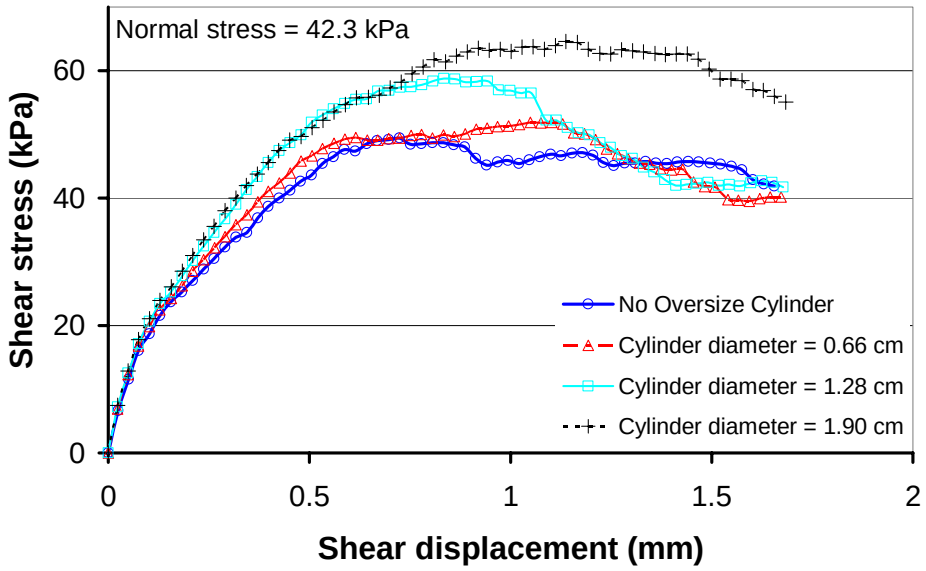

Figure B - 4: Shear stress vs. shear displacement of the numerical shear tests with the applied normal stress of 42.3 kPa for the oversize cylinder placed on the left side of the box.

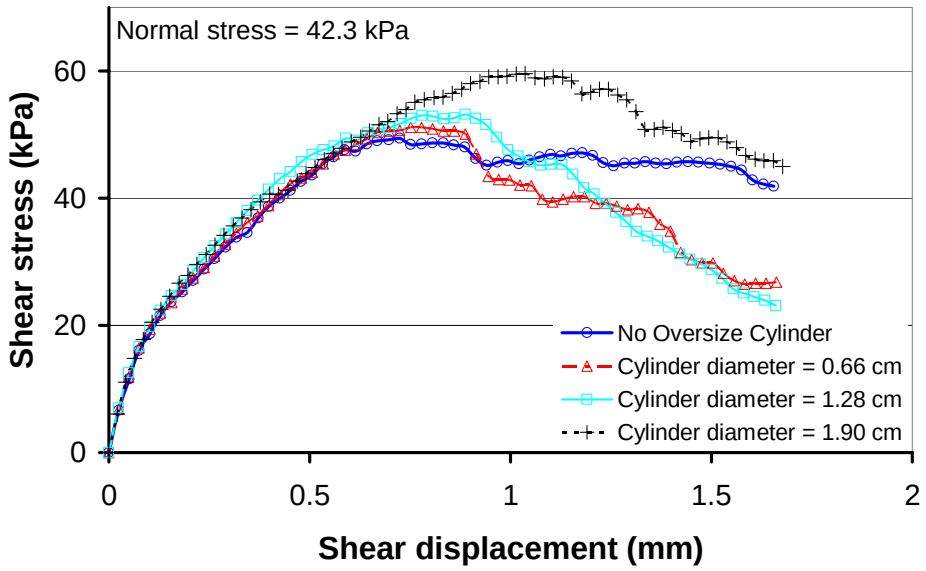

Figure B - 5: Shear stress vs. shear displacement of the numerical shear tests with the applied normal stress of 42.3 kPa for the oversize cylinder placed in the middle of the box.

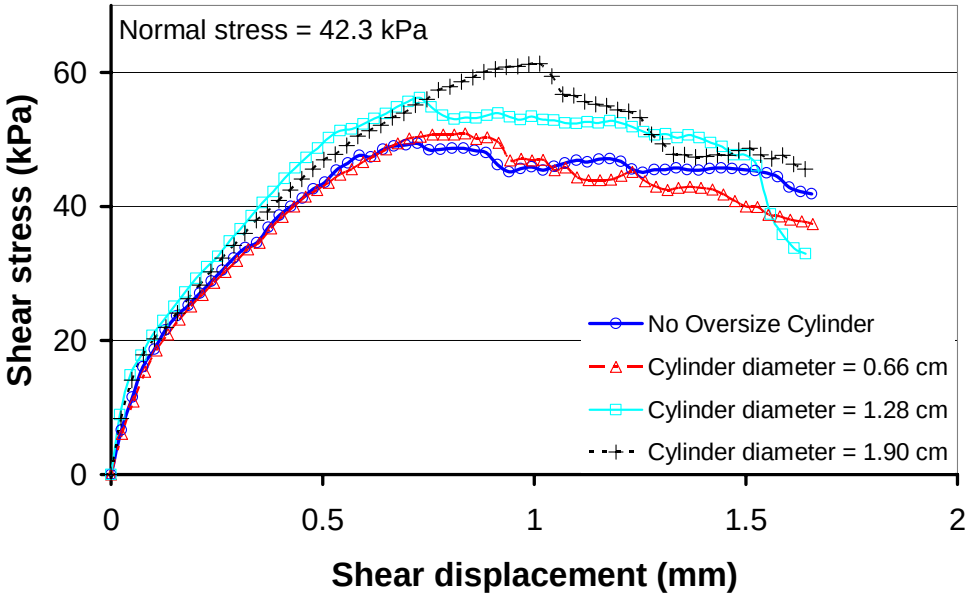

Figure B - 6: Shear stress vs. shear displacement of the numerical shear tests with the applied normal stress of 42.3 kPa for the oversize cylinder placed on the right side of the box.